CALCULATION OF STRESS INTENSITY FACTOR FOR AN EDGE CRACKED SHAPE MEMORY ALLOY PLATE

by

Sertan Alkan

B.S., Mechanical Engineering , Boğaziçi University, 2010

Submitted to the Institute for Graduate Studies in
Science and Engineering in partial fulfillment of
the requirements for the degree of
Master of Science

Graduate Program in Mechanical Engineering
Boğaziçi University

2013

CALCULATION OF STRESS INTENSITY FACTOR FOR AN EDGE CRACKED SHAPE MEMORY ALLOY PLATE

APPROVED BY:

Prof. Günay Anlaş (Thesis Supervisor)	.....
Assist. Prof. C. Can Aydıner	.....
Assist. Prof. Kutay Orakçal	.....

DATE OF APPROVAL: 06.20.2013

ACKNOWLEDGEMENTS

I would like to express my deeepest sense of gratitude to my thesis supervisor Prof. Günay Anlaş for his great support, advice, patience, and endless encouragement during this research. It has been an honor for me to work with him.

I would like to express my sincere gratitude to Assist. Prof. Can Aydıner and Assist. Prof. Kutay Orakçal for their support, interest and helpful comments in this thesis.

I am thankful to all faculty & staff members and my friends Erdem, Selçuk, Nima, Behrouz, Mustafa, Ayça, Kadri, Mete and all others who didn't hesitate to help when necessary.

Finally, I take this opportunity to thank my beloved parents and my brother for their love, support and motivation during all my life.

ABSTRACT

CALCULATION OF STRESS INTENSITY FACTOR FOR AN EDGE CRACKED SHAPE MEMORY ALLOY PLATE

In this thesis, the effect of martensitic transformation on stress intensity factor in an edge cracked shape memory plate loaded under Mode I conditions is studied. J contour integral is evaluated by an explicit technique and the results are compared to those of ABAQUS. It is seen that J integral is path dependent in martensite region at the crack tip. But, it remains path independent in austenic zone. Also a decrease in stress intensity factor due to martensitic transformation at the crack tip is observed. In addition to this, micromechanics based calculations in the literature are reviewed and modified to discuss the toughening effect as a result of phase transformation. Eshelby approach with a weight function method is utilized in order to quantify the decrease in stress intensity factor. Using analytical expressions from literature, transformation effect on stress intensity factor is also calculated. The orientation of crystals are taken into account by calculating variants and related transformation strains. The assigned orientation is seen to be responsible of difference in magnitude of stress intensity factor.

ÖZET

KENAR ÇATLAKLI ŞEKİL HAFIZALI ALAŞIM PLAKALARDA GERİLİM ŞİDDET ÇARPANININ BELİRLENMESİ

Bu tezde, martensitik faz dönüşümünün Mod-I yükleme altındaki kenar çatlaklı şekil hafızalı alaşım bir plakanın gerilim şiddet çarpanına etkisi çalışılmıştır. Bu amaçla, J integral değerleri haricen nümerik olarak hesaplanmış ve ABAQUS'ün kendi sonuçlarıyla karşılaştırılmıştır. J integralin çatlak ucundaki martensit bölgede yol bağımlı olduğu görülmüştür. Fakat östenitik bölgede yol bağımsız olmaya devam etmiştir. Ayrıca faz dönüşümü nedeniyle gerilim şiddet çarpanında azalma gözlenmiştir. Bunlara ek olarak literatürdeki mikromekanik bazlı hesaplamalar gözden geçirilmiş ve tokluk etkisini tartışmak amacıyla üzerlerinde değişiklik yapılmıştır. Gerilim şiddet çarpanındaki azalmayı belirlemek için ağırlık fonksiyonuyla birlikte Eshelby yaklaşımı kullanılmıştır. Literatürdeki analitik ifadelerden yararlanarak faz dönüşümünün gerilim şiddet çarpanı üzerindeki etkisi hesaplanmıştır. Kristallerin yönelim etkisi varyant ve ilgili faz dönüşüm uzanımlarıyla hesaba katılmıştır. Önceden belirlenen yönelimin gerilim stress çarpanının büyüklüğü üzerinde etkisi olduğu görülmüştür.

TABLE OF CONTENTS

LIST OF FIGURES

LIST OF TABLES

LIST OF SYMBOLS

a	Crack length
a_e	Effective crack length
A^{0f}	Austenite transformation finish temperature at zero stress state
A^{0s}	Austenite transformation start temperature at zero stress state
A^f	Austenite transformation finish temperature at prescribed equivalent stress state
A^s	Austenite transformation start temperature at prescribed equivalent stress state
A^*	Domain where area integral is evaluated
B	Width of the plate
b	Body force
b_M	Thermodynamic constant
C	Piecewise smooth curve
C^o	Celsius
C^A	Stress influence coefficent of austenite phase
C^M	Stress influence coefficent of martensite phase
cos	cosine function
exp	exponential function
E	Elastic modulus
E_A	Austenite phase elastic modulus
E_M	Martensite phase elastic modulus
E'	Effective elastic modulus for plane problem
E_{tip}	Elastic modulus value at the crack tip
f	Function
F	Dimensionless function
G	Rate of change of potential energy per unit crack advance area
GPa	GigaPascals

H	Height of the plate
h	Stress weighht function
J	J integral
J^*	J star integral
$\tilde{J}$	J tilde integral
K	Kelvin
K_{max}	Maximum stress intensity factor
K_I	Stress intensity factor for Mode I
K_{Ie}	Effective stress intensity factor
K_{II}	Stress intensity factor for Mode II
lim	Limit operator
m	meter
mm	milimeters
M	Martensite Phase
M^{0s}	Martensite transformation start temperature at zero stress state
M^{0f}	Martensite transformation finish temperature at zero stress state
M^f	Martensite transformation finish temperature at prescribed equivalent stress state
M^s	Martensite transformation start temperature at prescribed equivalent stress state
Md	Upper temperature limit of pseudoelastic behaviour
MPa	MegaPascals
N	Shape function
n	Unit exterior normal
P	Load
q	Smooth function representing translation of crack tip
r	Radial distance from crack tip
r^A	Boundary for fully austenite zone
r^M	Boundary for fully martensite zone
r^*	Transformation zone boundary

R_{Notch}	Notch geometry transformation zone boundary
$R_{1mmcrack}$	$1mm$ crack geometry transformation zone boundary
$R_{2mmcrack}$	$2mm$ crack geometry transformation zone boundary
s	Deviatoric stress component
$\dot{s}$	Deviatoric stress increment
sin	sine function
T	Traction
T	Temperature of the medium
T^o	Reference temperature
t	Thickness
u	Displacement
W	Elastic strain energy density function
w	Stress work
w^p	Plastic component of stress work

α	Angle between central axis of cone formed by non-smooth yield surface exterior normals and deviatoric stress increment
α^t	Isotropic themal expansion coefficent
α^*	Ratio between martensite and austenite elastic moduli
β	Semivertex angle of the cone
Γ	Piecewise smooth curve
δ	Angle between central axis of cone and plastic strain increment
Δ	Change in corresponding quantity
ϵ	Total strain tensor
$\dot{\epsilon}$	Strain increment
ϵ^e	Elastic strain
ϵ_L	Uniaxial transformation strain
ϵ^p	Plastic strain
$\dot{\epsilon^p}$	Plastic strain increment
ϵ^{tr}	Stress free transformation strain

ζ	Local coordinate system component
η	Local coordinate system component
θ	Angle defined in counter-clockwise direction with respect to symmetry axis x
ν	Poisson ratio
ξ	Martensite volume fraction
π	Pi number
σ	Stress tensor
$\dot{\sigma}$	Stress increment
σ^{eq}	Equivalent stress state
σ^{∞}	Far field applied tensile stress
σ^{M}	Stress in fully martensite zone
σ^{*}	Stress state in elastic domain
σ^{tr}	Uniaxial transformation stress boundary
Ω	Interaxial angle in lattice

LIST OF ACRONYMS/ABBREVIATIONS

2-D	Two Dimensional
ASTM	American Society for Testing and Materials
A	Austenite Phase
CPS8	Quadratic plane stress element
CT	Compact tension
DIC	Digital Image Correlation
LEFM	Linear Elastic Fracture Mechanics
SEM	Scanning Electron Microscope

1. INTRODUCTION

With the development of new materials, more challenging tasks for design and continuum mechanics emerge; in that sense robust models have to be developed. In this thesis, shape memory alloy specimen with an edge crack, having unit thickness, subjected to uniform tensile loading will be studied in 2-D. The geometry and loading of the specimen is given in Figure 1.1.

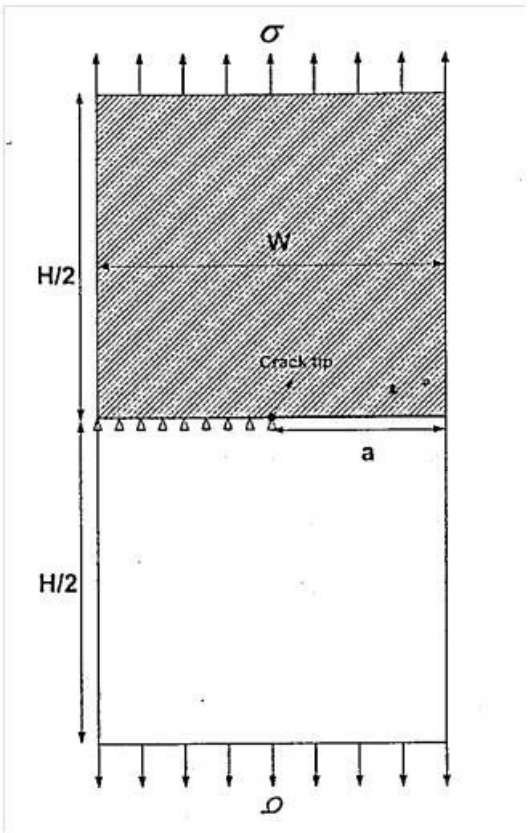

Figure 1.1. Load and crack geometry of Mode I [1].

Shape memory alloys are special alloys that exhibit martensitic transformation both thermally induced and stress induced. In thermally induced martensitic transformation, austenite phase (can be regarded as parent phase) transforms to martensite phase following certain class of thermodynamic paths due to the fact that different temperature ranges favor different crystallographic structures in terms of free energy.

In stress induced martensitic transformation, this crystallographic transformation is driven by stress as thermodynamical driving force at constant uniform temperature. NITINOL and Cu-AlZn are particular examples for these kind of materials that show martensitic transformation both thermally and stress induced. NITINOL is a generic name that is given to the family of alloys which are composed of various percentages of Ni and Ti. They were developed in 1961 during an examination of ten different intermetallic compounds for missile nose tip materials. The development of this noval alloys is recorded under US patent number of 3 174 851 and dated March 23 1965. The inventors, W.J. Buehler and R.C. Wiley, named the alloy family as NITINOL. This is derived from the chemical symbol NiTi and NOL is the acronym of "Naval Ordinance Laboratory " [2,3].

Shape memory alloys are subjected to only expected thermal contraction strains down to transformation temperature under zero load during cooling if initial phase is austenite. However, as the critical martensite start temperature is reached, austenite phase transforms into martensite gradually. When the martensite finish temperature is reached, the transformation ends. At this stage, crystal structure fully transforms to martensite phase. However, this transformation occurs in such a special manner that different regions of the crystal transform to different variants of martensite and as a result there is no macroscopic shape change. This phenomenon is called self-accomodation and martensite transformed as so is named as self-accomodated (twinned) martensite. If the crystal is deformed after this stage, it rearranges the variants and forms a new microstructure where one of the variants is favored in representative volume element. This phenomenon is called detwinning. If applied load is released at this stage, a significant amount of inelastic strain will be observed. However, when austenite start temperature is reached by heating, firstly thermal strain increases. Then the martensite phase starts to transform to austenite phase. As the austenite finish temperature is reached, transform ends and crystal structure fully transforms to austenite phase. The interesting phenomenon is that almost all of the strain, induced during martensite deformation, is recovered. This whole sequence of physical events is called shape memory effect. The temperature differences between forward transformation (A$\rightarrow$ M) and backward transformation (M $\rightarrow$ A) causes hysteresis. For more

information on hysteresis, please see references [4-7].

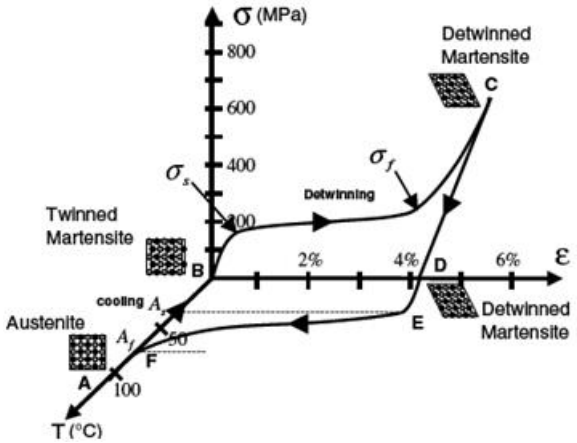

Figure 1.2. Stress–strain–temperature data illustrating shape–memory effect[4].

If the material is loaded mechanically by gradually increasing stress under constant temperature above austenite finish temperature, the phenomenon called stress induced transformation (superelasticity or pseudoelasticity) is observed. Firstly, it starts to deform linear elastically with elastic modulus of E_A. When martensite start stress state is reached, which is modeled differently by a variety of constitutive models, the martensite transformation starts. As the stress state becomes equal to martensite finish stress state, martensite volume fraction (ξ) gets equal to 1 and transformation is completed. Two phenomena occur simultaneously during this transformation stage. As the transformed martensite zones form twins similar to the thermally induced case, the applied stress state forces the representative volume of martensite to choose one of the variants. If loading proceeds to increase, the material behaves again linear elastically with E_M until yielding point. If applied load is gradually released, it follows the same path down to austenite start stress state and back transformation to austenite starts following a different path from the forward transformation. Then it reaches the austenite finish stress state and again deforms elastically with the same austenite elastic modulus. Since forward and backward transformation paths are different, hysteresis is observed during this phenomenon. And high magnitude of strains (5-6 %) can be recovered. If the temperature is above a critical temperature, although it is beyond austenite finish temperature, no transformation will be observed during loading. This

temperature is denoted as Md [4-7].

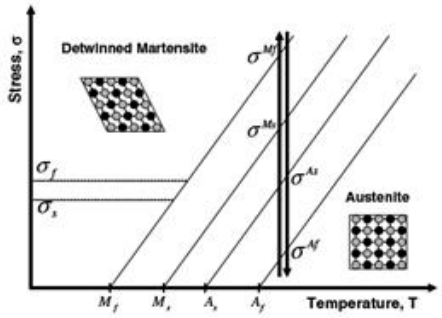

Figure 1.3. Stress–temperature graph of pseudoelastic effect [4].

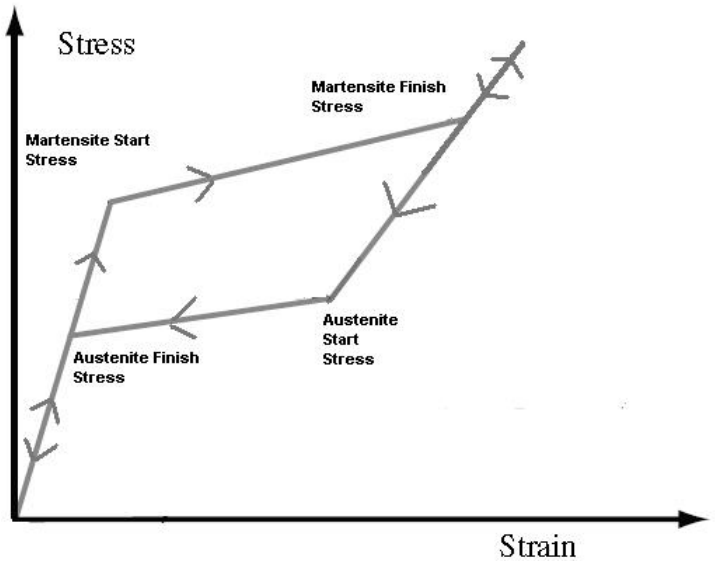

Figure 1.4. Stress-Strain graph of a shape memory alloy showing pseudoelasticity.

Transformation start and finish stresses depend on temperature. Equivalent stress expression is used in order to enclose multidimensional stress states. The relationships between transformation start-finish temperatures and equivalent stress states are given

by the following linear set of equations [4]:

$$M^s = M^{0s} + \frac{\sigma^{eq}}{C^M}$$
$$M^f = M^{0f} + \frac{\sigma^{eq}}{C^M}$$
$$A^s = A^{0s} + \frac{\sigma^{eq}}{C^A}$$
$$A^f = A^{0f} + \frac{\sigma^{eq}}{C^A}$$

where M^s, M^f, A^s, A^f are martensite start temperature, martensite finish temperature, austenite start temperature, austenite finish temperature respectively under a specific stress state. M^{0s}, M^{0f}, A^{0s}, A^{0f} are stress-free values of corresponding variables listed. σ^{eq} is equivalent stress state that depends on the constitutive model used. C^M and C^A are stress influence coefficents of martensite and austenite phases respectively. In the following parts of this chapter, a brief review of linear elastic fracture mechanics and related prominent literature is given. Following this, applications of the methods of fracture mechanics to shape memory alloys are listed which are found in the recent papers.

A crack in a solid can be loaded in three different modes or a combination of them. These can be classified as Mode I (opening mode), Mode II (sliding mode), Mode III (tearing mode). In Mode I, the displacements of the crack surfaces are perpendicular to the plane of the crack and normal stresses are applied. In Mode II type, in-plane shear is applied causing the displacements to stay in the plane of crack and perpendicular to the leading edge of the crack. And in Mode III due to out-of-plane shear, surface displacements are in the plane of crack and parallel to the leading edge of the crack.

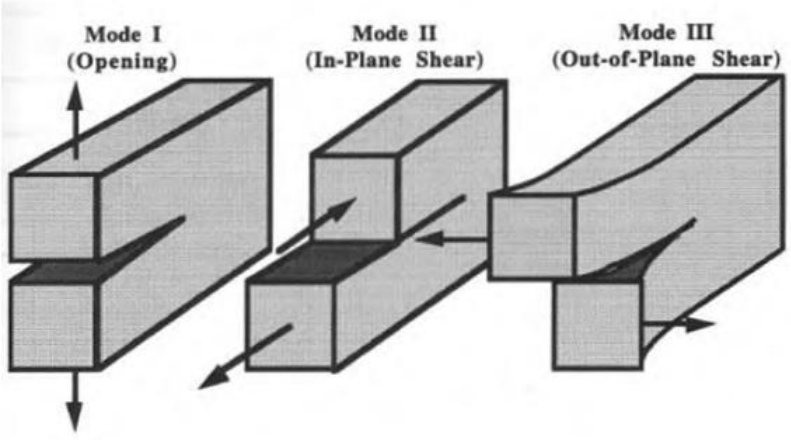

Figure 1.5. Different modes of loading that can be applied to a crack [8].

The stress distribution around a crack in Mode I loading for a linear elastic, homogeneous, isotropic material can be calculated by asymptotic equation of Williams [9]. The equation gets the following form around the crack tip as r approaches 0

$$\sigma_{ij} = \frac{K_I}{\sqrt{2\pi r}} f_{ij}(\theta) \tag{1.1}$$

where r and θ are evaluated emanating from the crack tip and in counterclockwise direction respectively. K_I is called stress intensity factor. The crack tip stresses for the problem in Figure 1.1 are given as:

$$\sigma_{xx} = \frac{K_I}{\sqrt{2\pi r}} cos\frac{\theta}{2} [1 - sin\frac{\theta}{2} sin\frac{3\theta}{2}] \tag{1.2}$$

$$\sigma_{yy} = \frac{K_I}{\sqrt{2\pi r}} cos\frac{\theta}{2} [1 + sin\frac{\theta}{2} sin\frac{3\theta}{2}] \tag{1.3}$$

$$\sigma_{xy} = \frac{K_I}{\sqrt{2\pi r}} cos\frac{\theta}{2} sin\frac{\theta}{2} cos\frac{3\theta}{2} \tag{1.4}$$

For large r values, the aforementioned stress formulation is inadequate since other terms of the series solution of Williams [9] are not going to be negligible and have to be taken into account. To relate outer applied loading to stress intensity factor at the

crack tip Westergaard's approach is used [10]. According to this

$$K_I = F(a, B)\,\sigma^{\infty}\,\sqrt{\pi a} \tag{1.5}$$

where σ^{∞}: far field applied stress, B is width of the plate and F is dimensionless function taking effect of finite size and geometry into account. As long as the modes of applied loadings are consistent , superposition principle can be used for combined loading.

When strain energy is a function of only strain state (not position or path history) Rice's J integral can be used for determination of stress intensity factor [11]. It's a line integral related to energy around the crack tip and is able to solve K_I even for some cases where plastically deformed zones are present under certain conditions such as proportional loading. J integral at the crack tip is equal to G which is rate of change of potential energy per unit crack advance area for elastic materials. Also, J integral is used as a fracture criterion under plane strain conditions since it is the critical case due to small inelastic deformation zone compared to plane stress. The form of this line integral for 2-D, elastic case ($i = 1, 2$) is as the following.

$$J = \int_C W dy - T_i \frac{\partial u_i}{\partial x} dS \tag{1.6}$$

In this expression, W is strain energy density per unit volume, C is piecewise smooth curve whose ends are at the crack faces, T_i is traction vector component for outward pointing surface bounded by C, and u_i is displacement component.

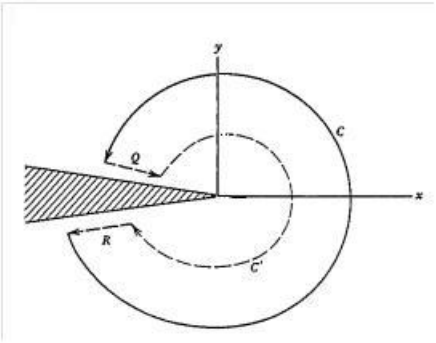

Figure 1.6. J integral closed contour illustration [12].

For the case of a linear elastic, isotropic, homogeneous material, J integral is zero if the C contour is a closed piecewise smooth curve and there is no singularity inside or on it (in the absence of body force, thermal strain and applied traction on the crack faces). The relationship between J integral and stress intensity factor K_I is:

$$J = \frac{K_I^2}{E'} \tag{1.7}$$

where

$$E' = E \quad for\ plane\ stress \tag{1.8}$$

$$E' = \frac{E}{1-\nu^2} \quad for\ plane\ strain \tag{1.9}$$

The material presented above discusses homogeneous materials. Eischen [13] showed that the nature of singularity of stress field for a nonhomogeneous elastic medium whose elastic modulus varies according to spatial coordinates (r,θ) is same as homogeneous media. He developed a path - independent J^* integral for isotropic , linear elastic materials whose material properties vary by a known distribution spatially. He also achieved to relate two contour integrals, named as J_1^* and J_2^* , to crack tip stress intensity factors in Mode I (K_I) and Mode II (K_{II}). The generic form of these integrals are given as:

$$J_k^* = \int_C \left(W n_k - \sigma_{ij} n_j u_{i,k} \right) dC \tag{1.10}$$

J_1^* has a well known physical meaning and is equal to rate of change of potential energy per unit crack advance area, G.

$$G = \int_C \left(W n_1 - \sigma_{ij} n_j u_{i,1} \right) dC = J_1^* \tag{1.11}$$

In this expression, n_1 is x component of unit normal vector to contour C traversing counterclockwise sense. The integrals, J_1^* and J_2^*, in terms of K_I and K_{II} are given in the expressions below. E_{tip} is elastic modulus value at the crack tip.

$$J_1^* = \frac{1}{E_{tip}}(K_I^2 + K_{II}^2) \quad for\ plane\ stress \tag{1.12}$$

$$J_2^* = \frac{1}{E_{tip}}(-2K_I K_{II}) \quad for\ plane\ stress \tag{1.13}$$

In 2000 for functionally graded materials Anlas, Santare and Lambros [14] developed a numerical implementation of path independent integral $\tilde{J}$ which is seen in the equation below. It is shown that this $\tilde{J}$ integral, the strain energy release rate G and $\lim_{r\to 0} J$ are numerically equal even for rather coarse meshes.

$$\tilde{J} = \int_\Gamma \left(W n_1 - \sigma_{ij} n_i \frac{\partial u_i}{\partial x} \right) dS - \int_A W_{,1}\, dA \tag{1.14}$$

In the equation above, Γ is any random path which begins at the bottom crack face and ends at the top crack face. A is the area enclosed by that contour. $W_{,1}$ indicates "explicit" partial differentiation of W with respect to x.

Fracture phenomenon of shape memory alloys has been discussed in a number of studies using experimental or numerical methods, recently. Gollerthan *et al.* [15] carried out experiments on NiTi in two type of compositions: 50.7% Ni pseudoelastic which is austenite at 295 K and 50.3% Ni which is martensite at 295 K. They tested these specimens having different compositions to find critical stress intensity factor for Mode I fracture , K_{max}. It is obtained by the formula below where P, B, t and a corresponds to applied load, specimen width, thickness of the specimen, and crack length induced by fatigue loading according to ASTM E 399 standard [16] respectively.

$$K_{max} = \frac{P}{t\sqrt{B}} f\left(\frac{a}{B}\right) \tag{1.15}$$

Compact Tension (CT) specimens having t=7.2 mm, B=16 mm and $\frac{a}{B}$ ratios varying between $0.45 - 0.55$ (which are sugggested ratios by ASTM E 399 [16]) gave the following results in the experiments:

Table 1.1. Maximum stress intensity factors measured by Gollerthan *et al.* [15].

Austenite (423 K)	53 MPa$\sqrt{m}$
Pseudoelastic (295 K)	34 MPa$\sqrt{m}$
Martensite (295 K)	31 MPa$\sqrt{m}$

As it is seen in the table above, austenite phase has higher resistance to fracture. Hence this data differ from classical plasticity where inelasticity at the crack tip increases material's resistance against crack propagation. Also, pseudoelastic and martensite specimens have similar values due to detwinned microstructure observed at both specimens. Gollerthan *et al.* observed slower crack propagation for martensite specimen in comparison to pseudoelastic and austenite specimens . Lastly they made synchtron measurements. This enabled them to detect martensite formation at the central plane of the specimen where plane strain conditions rule. It has been confirmed that under plane strain conditions martensite forms at the crack tip.

Daymond *et al.* [17] studied texture formation at the tip of a crack in martensitic NiTi CT specimen due to detwinning. They applied a nominal stress intensity factor $K = 35\text{MPa}\sqrt{m}$. They observed increase in (0 1 0) plane peak intensities, but decrease in (1 0 0) plane peak intensities by X ray diffraction experiments. They also compared the extent of the dewinned zone with Linear Elastic Fracture Mechanics (LEFM) predictions of the same geometry under plane strain conditions (Elastic Modulus = 62 GPa and Poisson's Ratio = 0.3). They took transformation equivalent stress as 200 MPa in average since detwinning transformation start and finish stresses are 150 MPa and 300 MPa respectively. This comparison of zone sizes leads to a qualitative agreement between test results and analytical approach, although there are ambiguities in such a comparison of an inelastic phenomena with linear elastic calculation. Also, significant compressive residual strain was detected near the crack tip after unloading.

Victor Birman [18] used William's stress formulation [9] to find transformation zone size at $\theta = 0$. In his method, firstly von Mises effective stress is written, then it is plugged into Tanaka 's martensite fraction formula [19]. Tanaka's formula is given below.

$$\xi = 1 - exp\left(b_M(M^{0s} - T) + \left(\frac{b_M}{C^M}\right)\sigma^{eq}\right) \tag{1.16}$$

$$b_M = \frac{ln(0.01)}{M^{0s} - M^{0f}} \tag{1.17}$$

Birman concluded that crack tip stress intensity factor is not much affected by the transformation. His results indicate that transformation toughening is significant when stresses in the martensite region is close to yield strength of the martensite phase. However; Birman addressed that this formulation causes violation of compatibility in austenite + martensite zone where both phases are present . In order to overcome this problem, he suggested to subdivide this zone into narrow sections and keep elastic modulus and fractions constant over each region.

Wang *et al.* [20] studied an implementation of Auricchio's superelastic model [21] in ABAQUS UMAT [22] for a CT specimen's crack tip martensite transformation. They used a standard notched specimen in addition to 2 precracked specimens (1 mm & 2 mm length cracked) with the following material properties as seen in the figure 1.7. Firstly they increased the load monotonically and after the load made a peak at 7500 N, they released the load till zero level. According to their finite element analysis results, the transformation zone sizes are sorted as $R_{Notch} < R_{1mmcrack} < R_{2mmcrack}$. The zone sizes are dependent on loading path as expected due to hysteresis. Interestingly , their results show that the martensite transformation zone sizes are not crack size dependent.

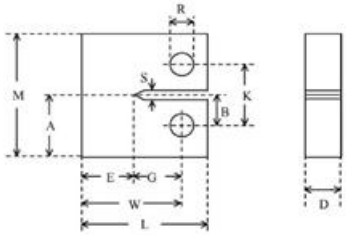

Fig. 2. CT specimen geometry.

Table 2
Dimenssons of the CT specimen shown in Fig. 2, in mm

Dimension	mm
L	20.0
M	19.2
D	8.0
E	8.8
G	7.2
W	16.0
S	1.6
R	4.0
K	8.8

Parameter	Symbol	Value
Elastic modulus	$E_{A,M}$	61 GPa
Stress where austenite starts forming on loading	σ_s^{AS}	529 MPa
End of stress plateau on loading	σ_f^{AS}	532 MPa
Stress where martensite starts forming on unloading	σ_s^{SA}	334 MPa
end of stress plateau on unloading	σ_f^{SA}	324 MPa
Extension of the stress plateau	ε_L	5%
	α	0

Figure 1.7. Dimensions of CT specimen and mechanical properties of shape memory alloy used by Wang *et al.* [20].

G.Z. Wang [23] studied the notch acuity effect on the transformation sizes and crack stability. He used an elastic-plastic constitutive ABAQUS finite element model. As a result of this study, it was shown that as the blunt notch converges to crack by increasing the acuity of the geometry, fully martensite zone increases. The partial transformation zones are similar for acute angle notch and crack, although blunt notch has a higher one. He also added plasticity effect to his finite element model and concluded that as the acuity of the notch increases, the fracture process zone at the crack tip decreases. This fracture zone is responsible for large strain zone inside the inelastically deformed martensite region. This result affects the stability of the crack propogation. As the acuity increases, the crack propagation stability changes from unstable to stable in contrast to traditional engineering materials.

Yi and Gao [24] proposed a method of calculating transformation toughening at the crack tip based on pseudoelastic model of Sun & Hwang [25,26] and Eshelby‘s inclusion method [27]. To simulate the effect of martensite transformation, cylindirical inclusions are used. They regarded the martensite phase transformation at the crack tip as discontinous in sense that they assumed no partial transformation outside the fully transformed process zone. They followed the same procedure as Evans *et al.* [28]

and used weight functions of Rice [29] to calculate the stress intensity factor induced by martensite inhomogeneity. As a result they concluded with the following formula:

$$\triangle K^{tip} = \frac{E}{1-2\nu}\int_A (\epsilon_{ij}^{tr} h_j)_{,i} dA \tag{1.18}$$

where ϵ_{ij}^{tr} is unconstrained transformation strain of martensite inhomogeneity. Weight function components are given in the following matrix equation.

$$\begin{bmatrix} h_1 \\ h_2 \end{bmatrix} = \frac{1}{2\sqrt{\pi}(1-\nu)\sqrt{r}} \begin{bmatrix} cos\frac{\theta}{2}(2\nu - 1 + sin\frac{\theta}{2}sin\frac{3\theta}{2}) \\ sin\frac{\theta}{2}(2 - 2\nu - cos\frac{\theta}{2}cos\frac{3\theta}{2}) \end{bmatrix} \tag{1.19}$$

The integral is evaluated over the transformed area. The following figure illustrates the tractions due to restriction of stress free transformation by surrounding medium.

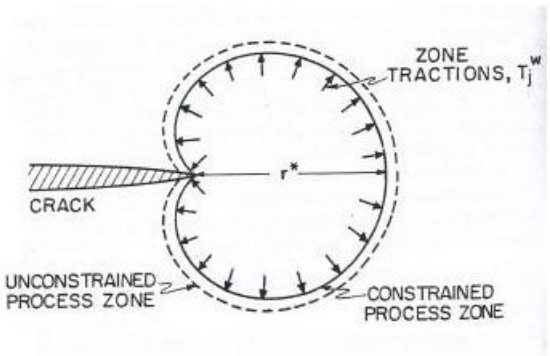

Figure 1.8. Tractions on tranformation zone due to constraining stress free transformation strain [28].

The transformed zone that is used in calculations is extracted from numerical solution in Yi and Gao's paper [24] where partial transforming zone is neglected. This decrease leads to toughening due to transformation. The following graph shows the effect of elastic moduli ratio on normalized stress intensity factor at 38^oC. K^∞ indicates stress intensity factor for a nontransforming material having same applied load and geometry.

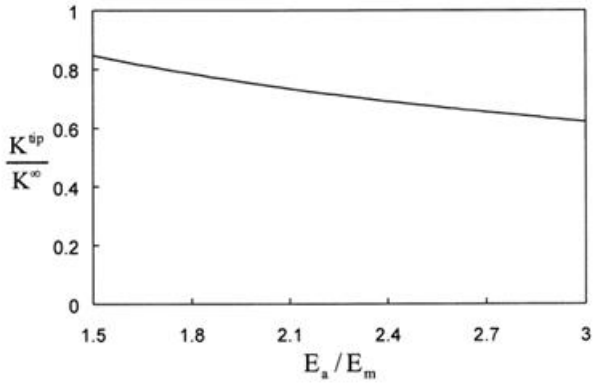

Figure 1.9. $\frac{E_a}{E_m}$ ratio effect on toughness in Yi and Gao [24].

In 2001, Yi *et al.* [30] extended the same the approach and studied mixed mode transformation toughening. They observed that in mixed mode problem transformation boundary is not symmetric in contrast with Mode I problem.

Yan *et al.* [31] investigated the effect of volume contraction depending on the data supplied by Fang *et al.* [32]. They took the trace of stress tensor as critical parameter for forward transformation and implemented a finite element model of quasi-advancing crack using ABAQUS. They drew attention to the increase in the stress intensity factor due to crack tip transformation although it is small in magnitude (0.39 % for NiTi and 0.37% for CuAlNi). This implies a transformation softening because of volume contraction at the crack tip.

Freed and Banks-Sills [33] published a paper approaching the problem from cohesive model point of view. They based their evaluations on the constitutive model of Panoskaltsis *et al.* [34] whose framework is a combination of general plasticity theory and continuum damage mechanics. They utilized path indepedency of J integral and claimed that stress intensity factor change is zero for quasistatic case. They determined transformation zone boundary from Panoskaltsis et al.'s transformation surface function which is von Mises type. Also, martensite start and finish surfaces are related by a normalized parameter. As a last point, a numerical implementation of crack propagation by a cohesive method is present in this paper. As the crack propagates, the

increase of cohesive traction induces an increase in steady state stress intensity factor for a fixed cohesive energy. This necessitates a higher magnitude of load for crack propagation.

Liefeng Ma addressed a solution based on Eshelby's inclusion method and Muskhelishvili's potentials in 2010 [35]. Although his method determines neither the extent of transformation zone nor the martensite fraction distribution in this zone, it evaluates the effect of transformation toughening analytically if these are obtained by means of other approaches. It can also be adapted for mixed mode crack tip problems.

Lexcellent and Thiebaud wrote a paper on the determination of transformation zone at the crack tip of a shape memory alloy in 2008 [36]. They used their own constitutive model based on plasticity [37-39] and William's asymptotic crack tip stress equations [9]. They tested the effect of a parameter concerning the asymmetry between tension and compression in their constitutive equations. However, they observed significant discrepancies between their analytical predictions and experimental results of Robertson *et al.* [40]. In 2011 Lexcellent, Laydi, and Taillebot extended the approach to mixed mode conditions [41].

An experimental work was carried out by Samantha Daly on NiTi sheet specimens using DIC (Digital Image Correlation) technique to observe the deformation field at the crack tip under Mode I conditions [42]. She claimed that strain could be expressed by $\frac{1}{\sqrt{r}}$ singularity in austenite zone at the crack tip and strain distribution along radial direction in partially transformed region is approximately linear. Lobes of martensite pointing at an angle of 60^o were observed at the crack tip. She also measured critical stress intensity factor for fine grained, polycrystalline, thin sheet NITINOL as 51.4 $\pm$ 3.6MPa. She used the model of Auricchio *et al.* [21] to implement finite element model of crack tip deformation. Her numerical results comply with the experimental observations such that in the austenite region strain field behaves as LEFM theory predicts. In the partially transformed zone, strain is linearly distributed.

As aforementioned, literature survey indicates that the studies carried on pseu-

doelastic transformation at crack tip does not give a strong mathematical insight. Experimental results are assessed using formulas directly related to linear elastic fracture mechanics of homogeneous materials. However, these evaluations give contrasting results on transformation toughening quantification. Rotation of principal axes due to transformation of austenite to martensite and reorientation of martensite may induce significant discrepancies from the classical methods of LEFM. The path dependency of J contour integral is an important question waiting to be answered since it is a powerful tool to evaluate stress intensity factor. Also numerical evalutions of principal axes rotations may give insight into the transformation and reorientation of phenomena at the crack tip.

This study aims to find a measure of transformation induced toughening at the crack tip. For this purpose, firstly, path dependency of J contour integral in shape memory alloys (in Auricchio *et al.*'s finite element model [21-22]) is discussed by explicitly calculating from output variables and utilizing ABAQUS inherent algorithm. Stress intensity factor obtained from explicit calculation of J integral will be presented. A method using weight function approach will be combined with Auricchio *et al.*'s finite element model [21-22] results and effect of transformation on stress intensity factor will be discussed. In addition, Eshelby approach will be extended by modelling martensite particles as spherical inclusions and using Mori-Tanaka approach [43]. Effect of texture on stress intensity factor in Mode I will be quantified using material properties published in the literature.

2. EFFECT OF TRANSFORMATION ON FRACTURE PARAMETERS

In this chapter, firstly, path dependency of J integral will be discussed. Auricchio *et al.*'s finite element model [21-22] was utilized in order to determine corresponding field variables and J integral values were extracted from ABAQUS for a single edge cracked specimen under plane stress for Mode I. In order to check the validty of J integral evaluation method in ABAQUS, J integral was also calculated by explicit formulation. Then stress intensity factor at the crack tip was quantified using J integral. Tri-linear model of Maletta *et al.* [50-52] is introduced and differences between two constitutive models are discussed in terms of proportionality of loading.

2.1. Numerical Evaluation of J Integral

Computation of J integral in numerical methods is paramount in problems containing cracks. The general expression for J integral taking thermal strains, plastic strains, body forces and traction applied on crack faces into account is given as the following expression below [8]:

$$J = \int_{A^*} \left(\left[\sigma_{ij} \frac{\partial u_j}{\partial x_1} - w\,\delta_{1i} \right] \frac{\partial q}{\partial x_i} + \left[\sigma_{ij} \frac{\partial \epsilon_{ij}^p}{\partial x_1} - \frac{\partial w^p}{\partial x_1} + \alpha^t \sigma_{ii} \frac{\partial T}{\partial x_1} - b_i \frac{\partial u_j}{\partial x_1} \right] q \right) dA ... \\ ... - \int_{\Gamma^+ \, \Gamma^-} \sigma_{2j} \frac{\partial u_j}{\partial x_1} \, q \, d\Gamma \tag{2.1}$$

Here in this notation w, w^p, ϵ_{ij}^p, α^t, b_i, and A^* are stress work, plastic part of stress work, plastic strain component, isotropic thermal expansion coefficent, body force component and the dashed area in the figure below enclosed by $\Gamma_- + \Gamma_1 + \Gamma_+ + \Gamma_0$ respectively. "q" variable will be discussed in detail below. The total strain components (ϵ_{ij}) are considered to be the sums of elastic strain components (ϵ_{ij}^e) and plastic strain

components (ϵ_{ij}^{p}).

$$\epsilon_{ij} = \epsilon_{ij}^{e} + \epsilon_{ij}^{p} \tag{2.2}$$

Total stress work is defined as:

$$w = \int_{0}^{\epsilon_{ij}} \sigma_{kl} d\epsilon_{kl} \tag{2.3}$$

Elastic strain energy density per unit volume is described by the following equation.

$$W = \int_{0}^{\epsilon_{ij}^{e}} \sigma_{kl} d\epsilon_{kl}^{e} \tag{2.4}$$

Then one can find w^p as the following by using deviatoric components, s_{ij}, of stress tensor, σ_{ij}:

$$s_{ij} = \sigma_{ij} - \frac{1}{3}\sigma_{kk}\delta_{ij} \tag{2.5}$$

$$w^{p} = w - W = \int_{0}^{\epsilon_{ij}^{p}} s_{kl} d\epsilon_{kl}^{p} \tag{2.6}$$

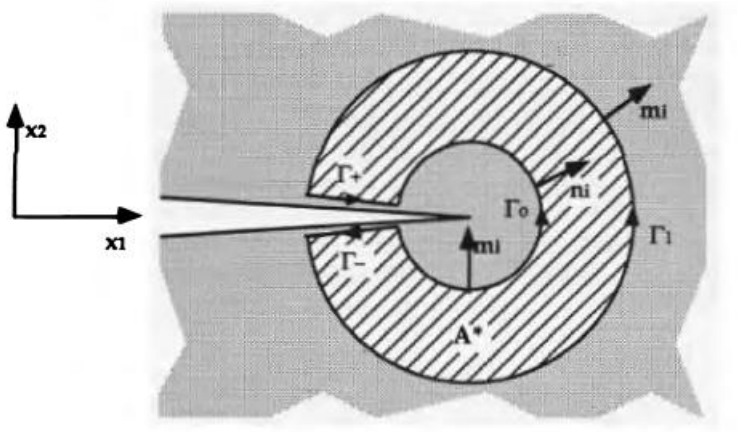

Figure 2.1. J contour integral schematic [8].

In the integral description above, "q" represents rigid body translation of nearby points to crack tip introduced by virtual crack extension method of Hellen [44-45], Parks [46], and DeLorenzi [47]. The common convention used takes $q = 1$ at the inner contour and $q = 0$ at the outer contour. Two common "q" functions assigned between the two contours can be seen in the figure below. In this figure first configuration (pyramidal) corresponds to linear change between the inner and outer contours while the second configuration (plateau) stays equal to 1 until the last ring of elements. Shih *et al.* [48] have shown that the computed values of J integral are insensitive to the assumed shape of "q" function.

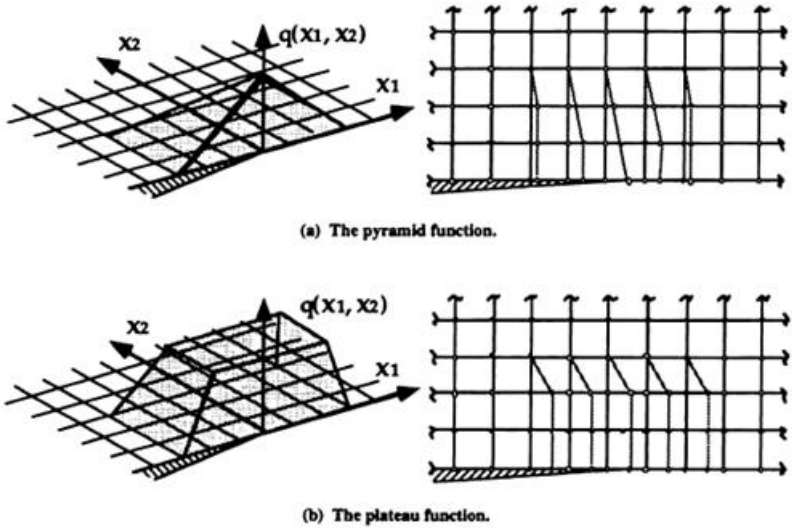

Figure 2.2. Commonly used q function configurations (i)Pyramidal (ii)Plateau [8].

The field variables inside the J integral can be extracted from resulting data of finite element analysis. However, "q" function is defined at the nodes. The node values are used to form "q" function inside each element similar to displacement field function generated inside each element by using nodal displacement values. The domain integral is evaluated by Gauss quadrature scheme according to the integration point number used in the elements. The values of "q" function inside the element can be interpolated by the following expression.

$$q(\zeta, \eta) = \sum_{i=1}^{n} N_i(\zeta, \eta) q_i \tag{2.7}$$

In the expression above, n value represents the number of element nodes, q_i are numerical values of "q" function at the corresponding nodes, $N_i(\zeta, \eta)$ are shape functions defined in local coordinates ζ and η . The relation between local coordinates (ζ , η) and physical, global coordinates (x , y) are given in the following equations where x_i is x coordinate of i^{th} node and y_i is y coordinate of i^{th} node.

$$x = \sum_{i=1}^{n} N_i(\zeta, \eta) x_i \tag{2.8}$$

$$y = \sum_{i=1}^{n} N_i(\zeta, \eta) y_i \tag{2.9}$$

In our problem, there is no applied traction on the crack surfaces. Hence only area integral in the generic J integral expression is considered without body forces and thermal incompabilities. Also, transformation strain is plugged in as plastic strain variable. ABAQUS software calculates J integral such that inner contour always stays sessile at the crack tip node. For each increment of outer contour, an extra ring of elements is enclosed by integral domain. The following figures show how ABAQUS evaluates J integral by moving outer boundary of the domain.

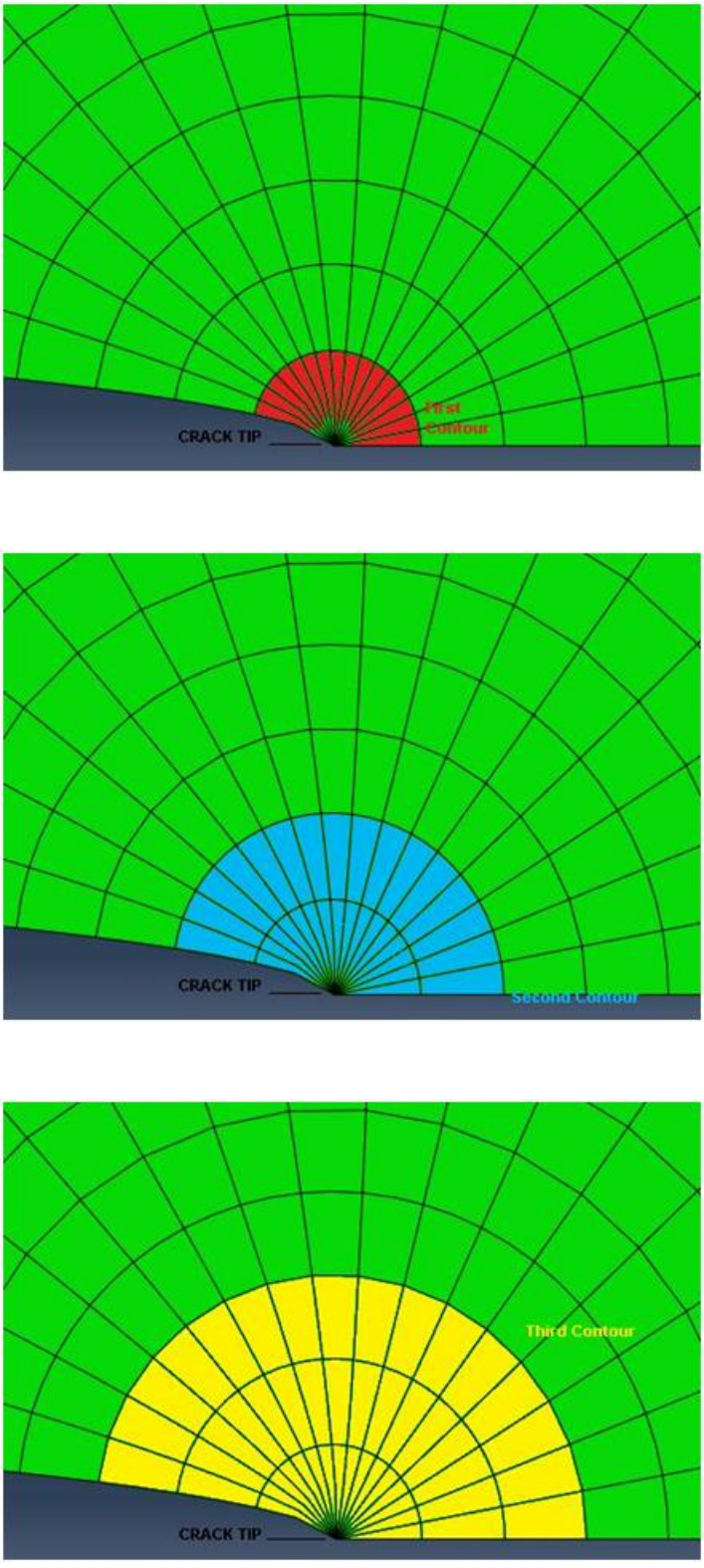

Figure 2.3. J integral evaluation for each contour by using domain integral approach in ABAQUS.

The main drawback of conventional ABAQUS J integral evaluation method is that it does not include the possibility of material property change inside an element as observed in the case of shape memory alloys on account of martensitic phase change. In this type of materials, the spatial distribution of martensite volume fraction ξ is not known before solving the full field boundary value problem. And the resulting martensite volume fraction may vary inside the elements near the crack tip. J integrals are calculated from a mixture of elements consisting austenite phase and martensite phase partially that do not allow to have an idea about the material property effect on J integral values. In order to overcome this obstacle, integration point data were extracted in fully martensite and austenite zones. The integration points were connected with line segments in order to form piecewise smooth contours. Hence the area integral was converted to path integral . Trapezoidal integrating scheme was used in order to calculate the integral between consecutive integration points where the path passes. In this analysis, ABAQUS quadratic plane stress element type (CPS 8) was used. The figures below show the positions of integration points on this element and how contours were taken in half model without restriction of ring formation.

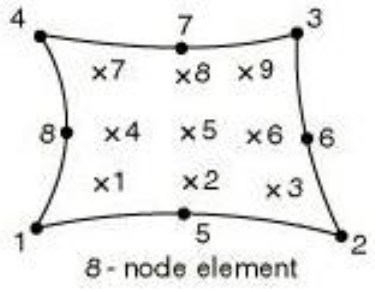

Figure 2.4. Schematic showing 8 node element's integration point and node locations.

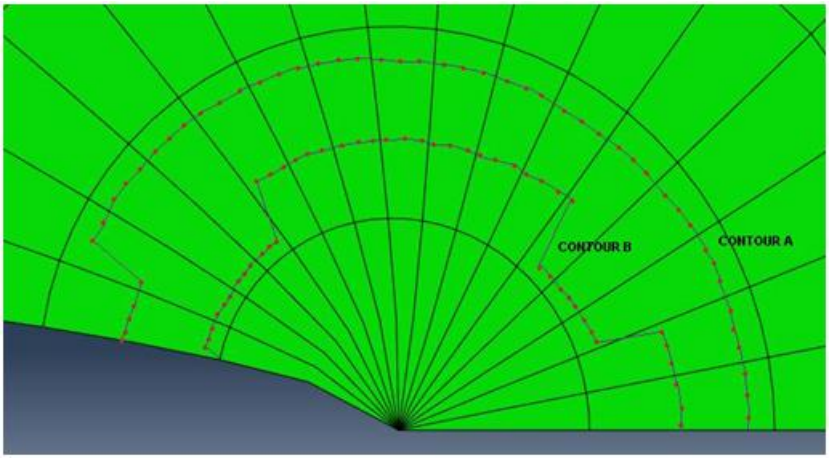

Figure 2.5. Sample of contours for explicitly J integral evaluation in half model.

The material parameters used in Auricchio *et al*'s finite element model [21-22] are listed in the table below. The model in the analysis was run at constant temperature of 295 K.

Table 2.1. Material properties used in ABAQUS Auricchio *et al.*'s model [21-22].

Elastic Modulus Austenite	75 GPa
Elastic Modulus Martensite	28 GPa
Poisson Ratio for both Martensite and Austenite	0.33
C^A Austenitic stress influence coefficent	5.71 $\frac{MPa}{^oC}$
C^M Martensitic stress influence coefficent	5.71 $\frac{MPa}{^oC}$
Martensite Start Stress (295 K)	400 MPa
Martensite Finish Stress (295 K)	410 MPa
Transformation Strain (Forward-Backward)	4%
Austenite Start Stress (295 K)	310 MPa
Austenite Finish Stress (295 K)	300 MPa
Volumetric Transformation Strain	4%

The model geometry can be seen in the figure below. To make use of the symmetry with respect to x axis, half of the geometry is modeled and the results from operations implemented on related data are modified whenever necessary to take account whole geometry of the problem.

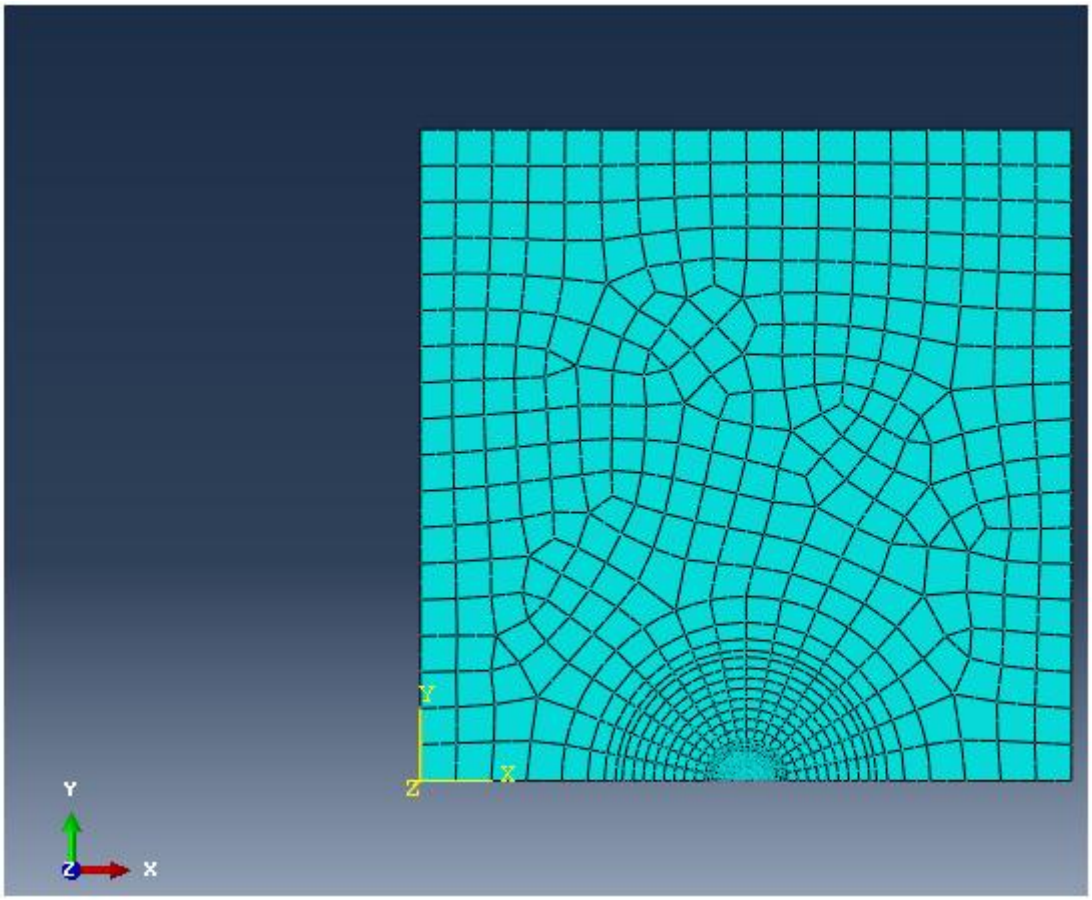

Figure 2.6. A schematic of mesh used in ABAQUS finite element analysis.

Firstly an edge cracked specimen having specimen width B = 100 mm and crack length a = 50 mm subjected to load in y direction σ^{∞} = 50 MPa at far field was analysed. J integrals below were evaluated in fully transformed martensite zone at the crack tip.

Table 2.2. J integral values for $\sigma^{\infty} = 50$ MPa and $\frac{a}{B} = 0.5$ in fully martensite zone from ABAQUS.

Contour Number	**J integral Value** $\left[\frac{N}{m} \right]$
1	48170
2	47600
3	47430
4	47090
5	46650
6	46140
7	45620

Table 2.3. J integral values for $\sigma^{\infty} = 50$ MPa and $\frac{a}{B} = 0.5$ in fully martensite zone.

Contour Number	**J integral Value** $\left[\frac{N}{m} \right]$
1	54017.2
2	53521.1
3	53305.9
4	52906.5
5	52607.4
6	52343.1
7	52183.5
8	52059.7
9	51889.0
10	51844.3
11	51751.4
12	51667.8
13	51647.7
14	51611.6
15	51345.9
16	51590.3
17	51576.5
18	51579.5
19	51371.9
20	52632.7
21	50434.7
22	51850.0
23	52498.1
24	52278.3
25	50823.4
26	49859.5

Standard deviation of explicitly evaluated J integrals in the table above is 903.4 $\frac{N}{m}$. The contours on which these integrals were evaluated are shown in the following figures.

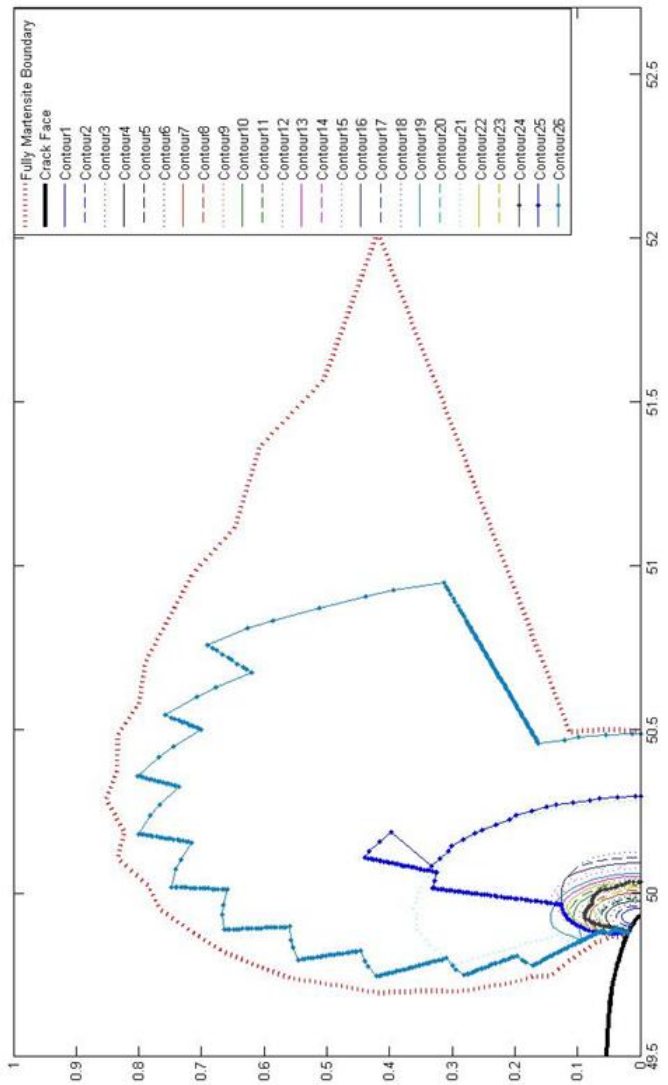

Figure 2.7. 26 contour paths taken in fully transformed martensite zone for $\sigma^{\infty} = 50$ MPa , $\frac{a}{B} = 0.5$.

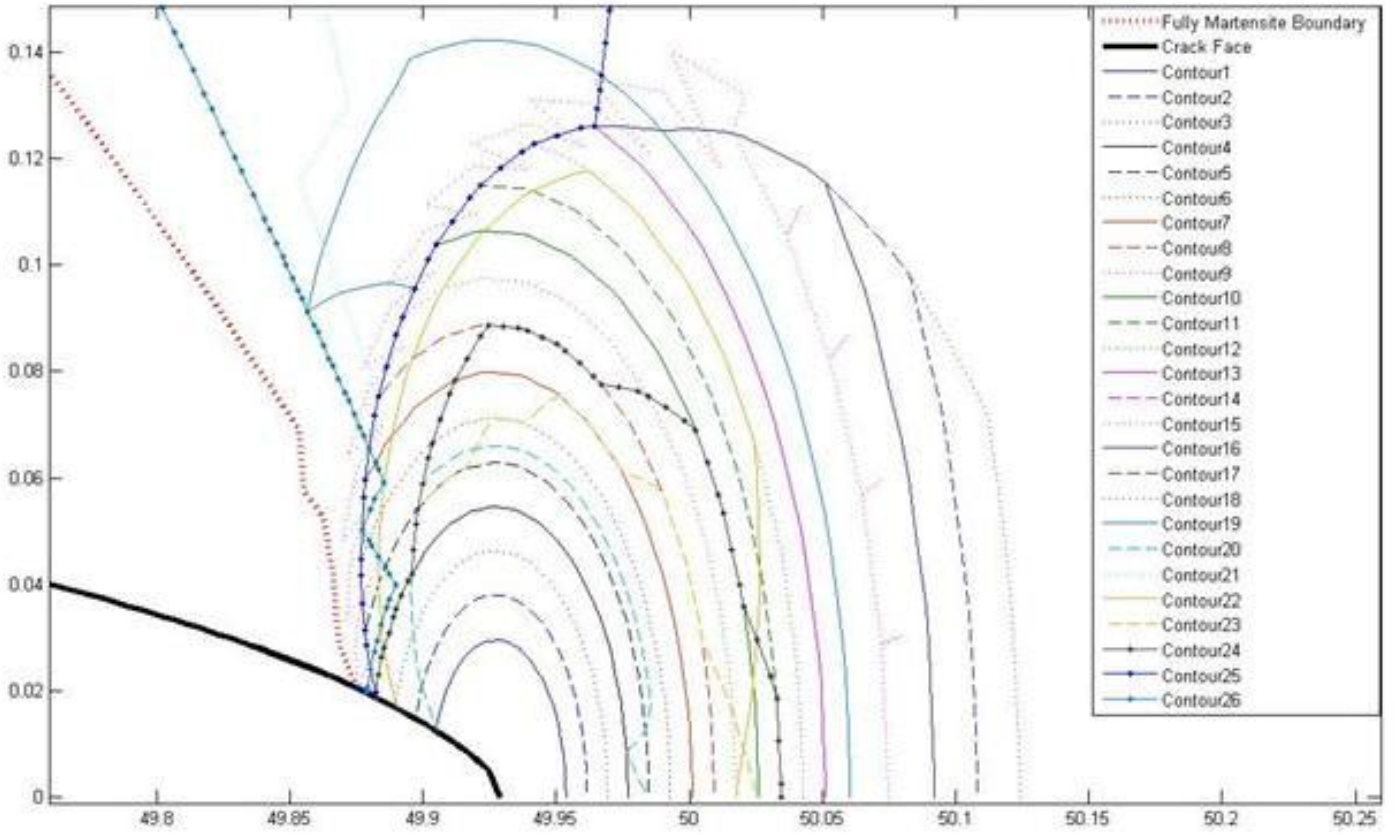

Figure 2.8. Closer view of 26 contours in fully transformed martensite zone for $\sigma^{\infty} = 50$ MPa, $\frac{a}{B} = 0.5$.

The following contour integrals were evaluated in the fully austenite zone.

Table 2.4. J integral values for $\sigma^{\infty} = 50$ MPa and $\frac{a}{B} = 0.5$ in fully austenite zone from ABAQUS.

Contour Number	**J integral Value** $\left[\frac{N}{m} \right]$
1	48040
2	48040
3	48040
4	48040
5	48040
6	48040
7	48040

Table 2.5. J integral values for $\sigma^{\infty} = 50$ MPa and $\frac{a}{B} = 0.5$ in fully austenite zone.

Contour Number	**J integral Value** $\left[\frac{N}{m} \right]$
1	48457.2
2	48511.7
3	48360.4
4	48729.7
5	48689.6
6	48692.4
7	48637.6
8	48537.8
9	48816.7
10	47946.9
11	48117.1

Standard deviation of the explicitly evaluated J integrals above is 268.39 $\frac{N}{m}$. The contours of these integrals can be seen in the figure below.

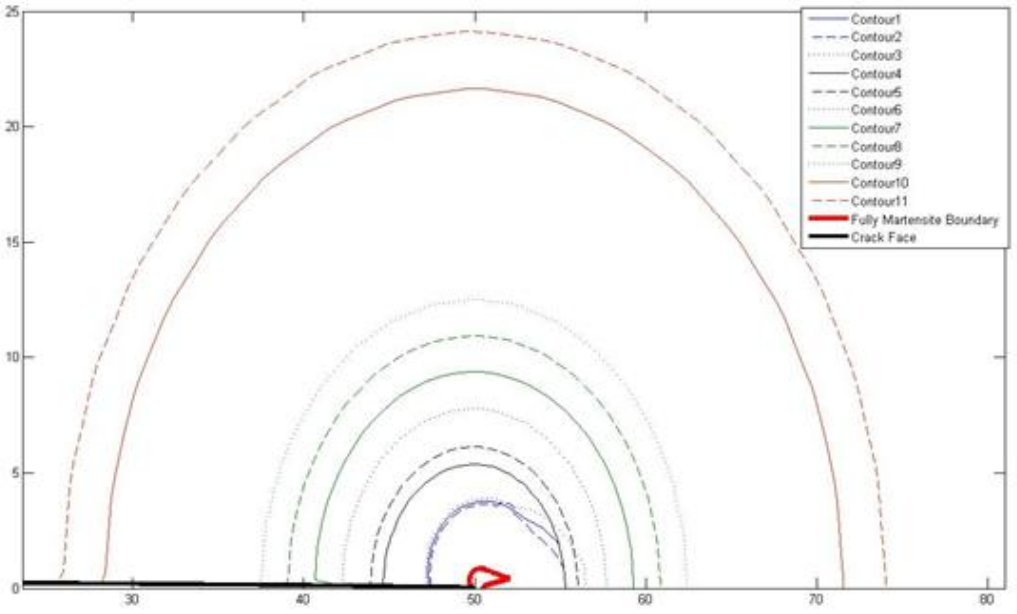

Figure 2.9. 11 Contours of J-integral evaluated in austenite zone for $\sigma^{\infty} = 50$ MPa, $\frac{a}{B} = 0.5$.

The next analysis is carried on a specimen having the same geometric dimensions but only changing $\sigma^{\infty} = 30$ MPa. Since fully transformed region is smaller in size, less number of contours can be taken in the fully martensite zone. The values are listed in the following tables.

Table 2.6. J integral values for $\sigma^{\infty} = 30$ MPa and $\frac{a}{B} = 0.5$ in fully martensite zone from ABAQUS.

Contour Number	**J integral Value** $\left[\frac{N}{m} \right]$
1	15600
2	15550

Table 2.7. J integral values for $\sigma^{\infty} = 30$ MPa and $\frac{a}{B} = 0.5$ in fully martensite zone.

Contour Number	**J integral Value** $\left[\frac{N}{m} \right]$
1	17862.8
2	17302.7
3	16993.7
4	17170.3
5	17021.2
6	16891.2
7	17105.9
8	16594.7
9	16906.4
10	16806.8
11	16551.7

Standard deviation of the explicitly evaluated J integrals above is 356.4 $\frac{N}{m}$. J integrals evaluated in the fully austenite zone are as the following:

Table 2.8. J integral values for $\sigma^{\infty} = 30$ MPa and $\frac{a}{B} = 0.5$ in fully austenite zone from ABAQUS.

Contour Number	**J integral Value** $\left[\frac{N}{m} \right]$
1	15720
2	15720
3	15720
4	15720
5	15720
6	15720

Table 2.9. J integral values for $\sigma^{\infty} = 30$ MPa and $\frac{a}{B} = 0.5$ in fully austenite zone.

Contour Number	**J integral Value** $\left[\frac{N}{m} \right]$
1	15737.8
2	15932.5
3	15917.0
4	15883.2
5	15948.5
6	16009.2

Standard deviation of the explicitly evaluated J integrals above is 91.74 $\frac{N}{m}$. The contours on which these set of path integrals were taken, can be viewed in the following two figures.

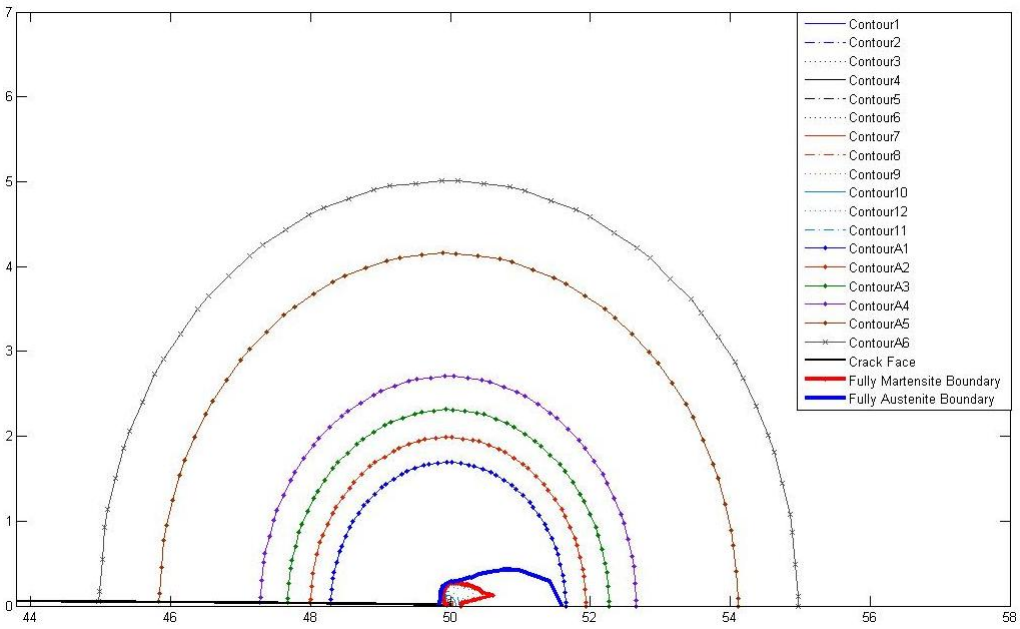

Figure 2.10. Contours taken both inside fully austenite region (6 contours) and fully martensite region (12 contours) for $\sigma^{\infty} = 30$ MPa, $\frac{a}{B} = 0.5$.

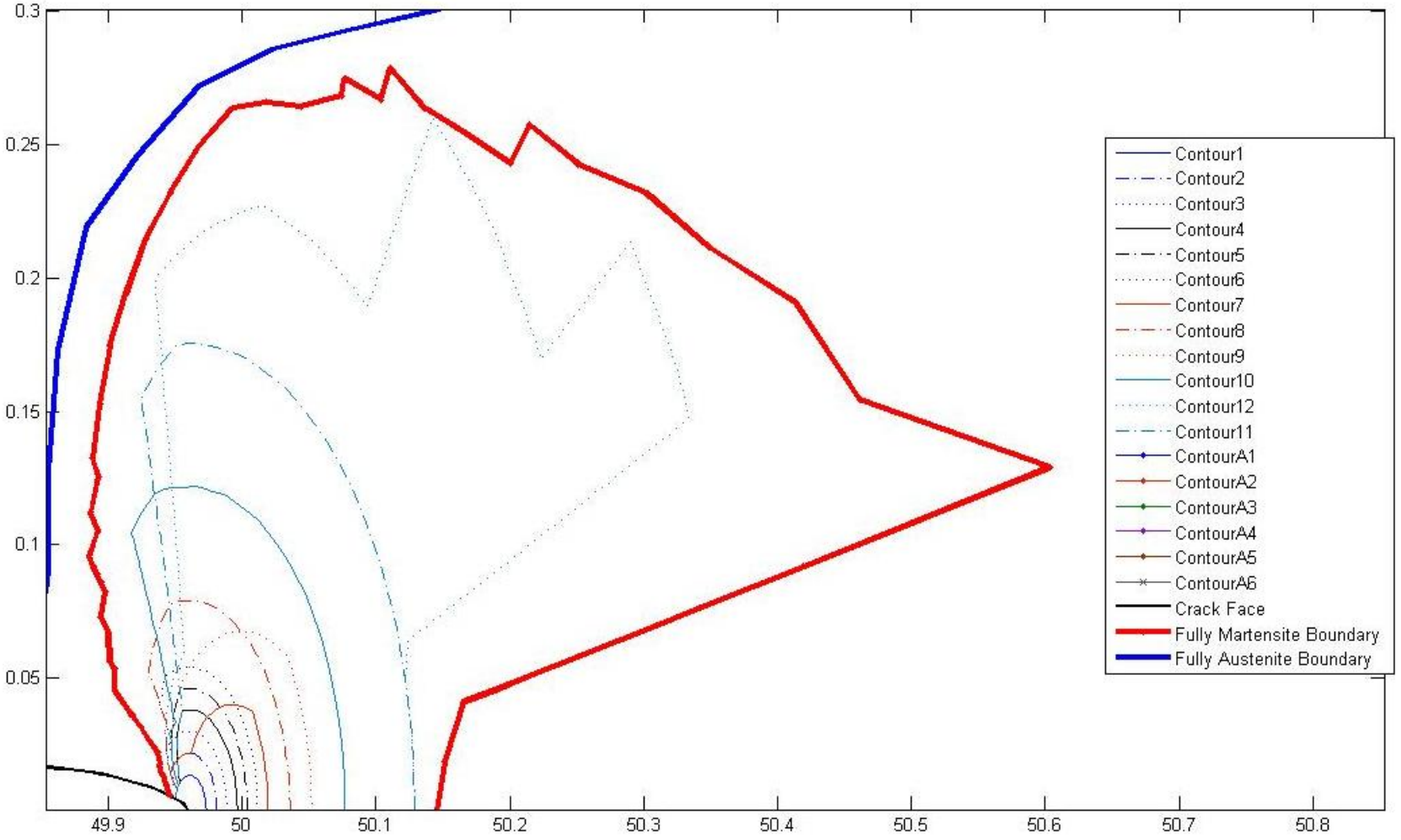

Figure 2.11. Detailed view of 12 contours taken both inside fully martensite region (12contours) for $\sigma^{\infty} = 30$ MPa, $\frac{a}{B} = 0.5$.

In order to see the effect of elastic constant change apart from transformation strain, fixed martensite elastic properties were assigned to the elements which were observed to be fully martensite in the previous finite element analysis for $\sigma^{\infty} = 50$ MPa far field loading case. The contour values in the fully martensite assigned zone are listed in the following table.

Table 2.10. Integral values for $\sigma^{\infty} = 50$ MPa and $\frac{a}{B} = 0.5$ in fully martensite assigned zone.

Contour Number	**J integral Value** $\left[\frac{N}{m} \right]$
1	44346.7
2	44773.4
3	44838.3
4	44834.1
5	44772.6
6	44693.0
7	44633.6
8	45784.6
9	44468.3
10	44619.6
11	44110.0
12	42864.1
13	44228.0
14	44676.0
15	44716.3
16	44713.8

The standard deviation of the explicity evaluated J integrals above is $581.5\frac{N}{m}$. J integral values in the fully austenite region can be found in the following table.

Table 2.11. Integral values for $\sigma^{\infty} = 50$ MPa and $\frac{a}{B} = 0.5$ in austenite section assigned zone.

Contour Number	**J integral Value** $\left[\frac{N}{m} \right]$
1	43392.5
2	43547.5
3	43545.9
4	43532.5
5	43529.1
6	43515.6
7	43497.5
8	43429.5
9	43422.0
10	43391.1
11	43358.8

Standard deviation of the explicitly evaluated J integrals above is 71.08 $\frac{N}{m}$. The results in both zones can be taken as constant. The contours on which J integrals were evaluated are shown in the next two figures.

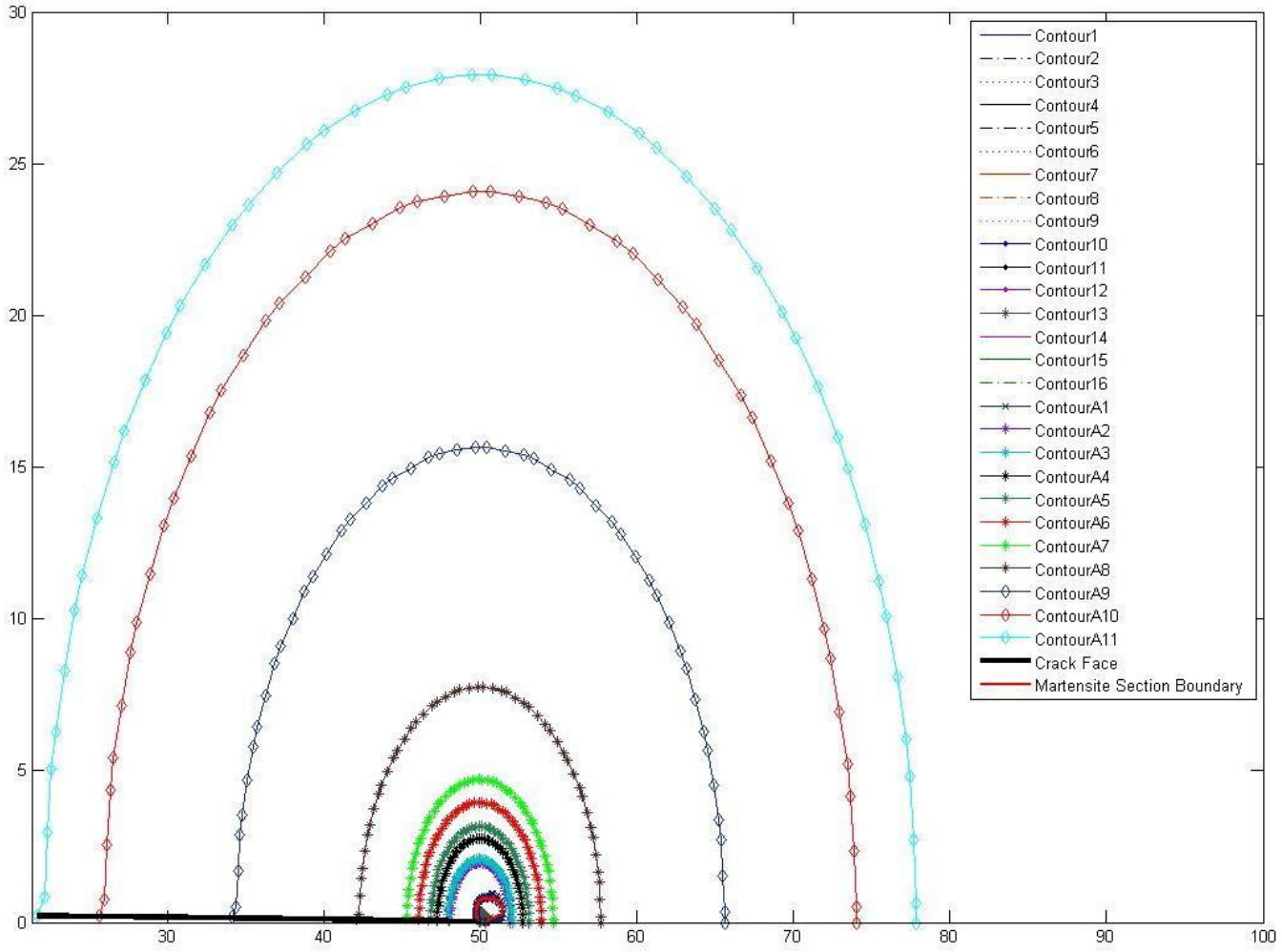

Figure 2.12. 16 contours inside martensite assigned section and 11 contours taken inside fully austenite zone for $\sigma^{\infty} = 50$ MPa, $\frac{a}{B} = 0.5$.

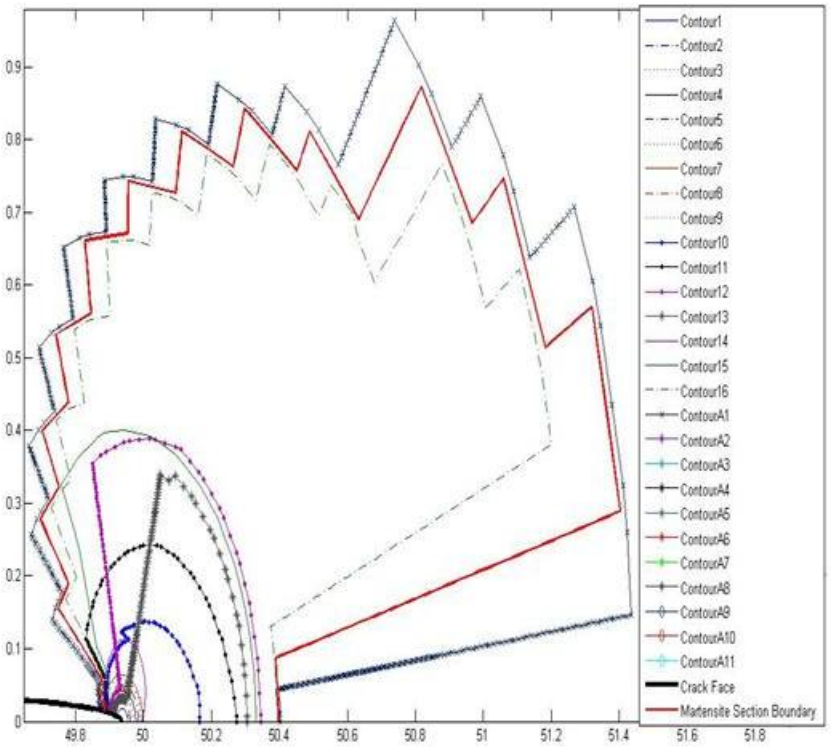

Figure 2.13. Closer view of 16 contours inside martensite assigned section for $\sigma^{\infty} = 50$ MPa, $\frac{a}{B} = 0.5$.

As expected in the fully austenite regions explicitly evaluated J integral values are nearly constant. Calculations of J integral by inherent ABAQUS algorithm also indicates constant values in the fully austenite. However, in the fully martensite regions J integrals seem to be changing on different contours. In order to check for the confirm this behaviour, the mesh size is decreased by half and re-run for $\frac{a}{B} = 0.5$ and $\sigma^{\infty} = 50$ MPa. The results are tabulated below for fully martensite zone and fully austenite zone.

Table 2.12. Integral values for 2 times refined mesh around crack tip $\sigma^{\infty} = 50$ MPa and $\frac{a}{B} = 0.5$ in fully martensite zone.

Contour Number	**J integral Value** $\left[\frac{N}{m} \right]$
1	59685.8
2	56669.0
3	56368.2
4	54469.8
5	54278.5
6	53012.0
7	52689.0
8	53027.0

Table 2.13. Integral values for 2 times refined mesh around crack tip $\sigma^{\infty} = 50$ MPa and $\frac{a}{B} = 0.5$ in fully austenite zone.

Contour Number	**J integral Value** $\left[\frac{N}{m} \right]$
1	48713.2
2	48703.7
3	48623.0
4	48707.1
5	48573.5
6	49030.9
7	48325.6
8	48002.4
9	48095.6

The standard deviation values for contours taken in fully martensite and fully austenite zones are 2888.8 $\frac{N}{m}$ and 328.9 $\frac{N}{m}$, respectively. The following two figures show contours on which J integrals were evaluated.

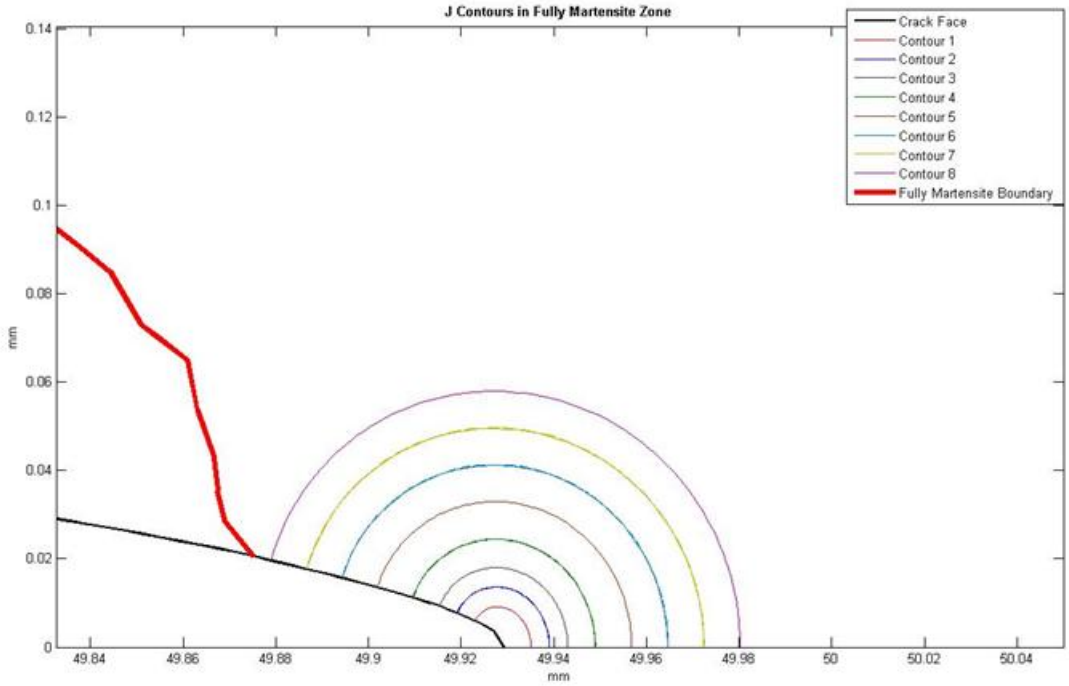

Figure 2.14. Integral contours for 2 times refined mesh around crack tip $\sigma^{\infty} = 50$ MPa and $\frac{a}{B} = 0.5$ in fully martensite zone.

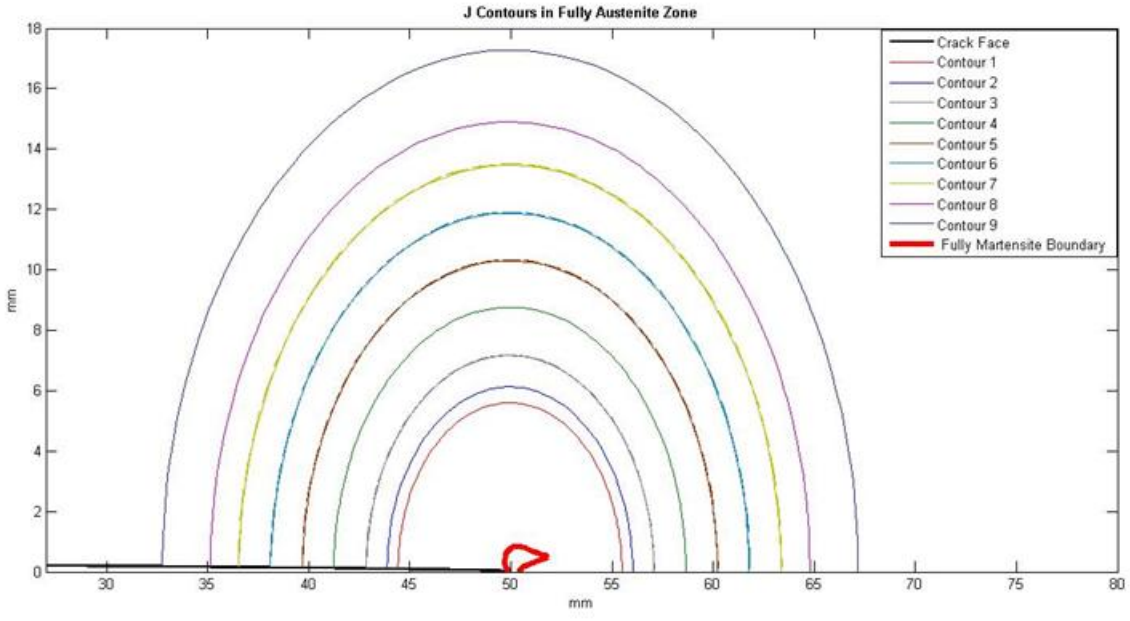

Figure 2.15. Integral contours for 2 times greater number of mesh around crack tip $\sigma^{\infty} = 50$ MPa and $\frac{a}{B} = 0.5$ in fully austenite zone.

The following 8 figures show the J integral values introduced in the above tables.

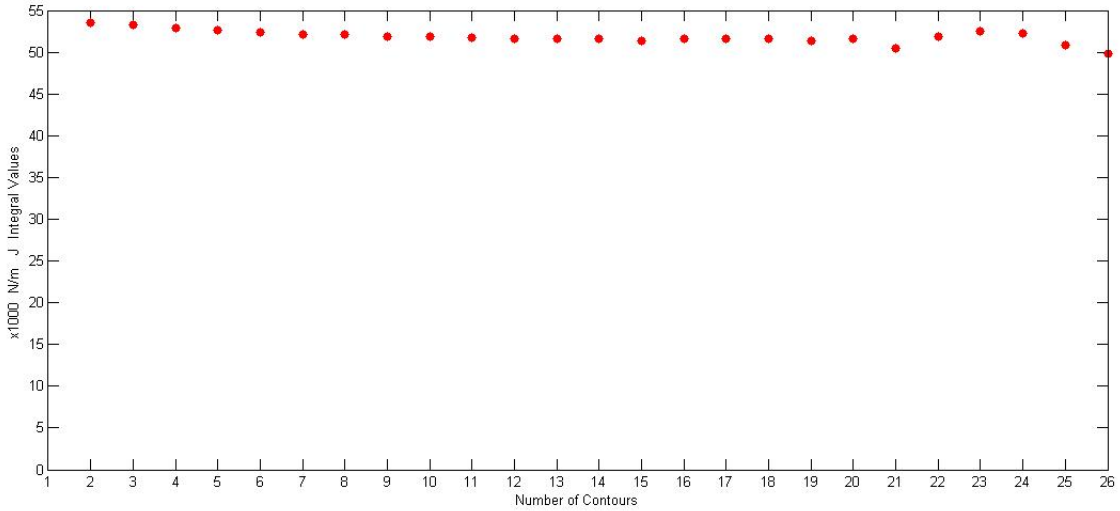

Figure 2.16. J integral values for $\sigma^{\infty} = 50$MPa, $\frac{a}{B} = 0.5$ in fully martensite region.

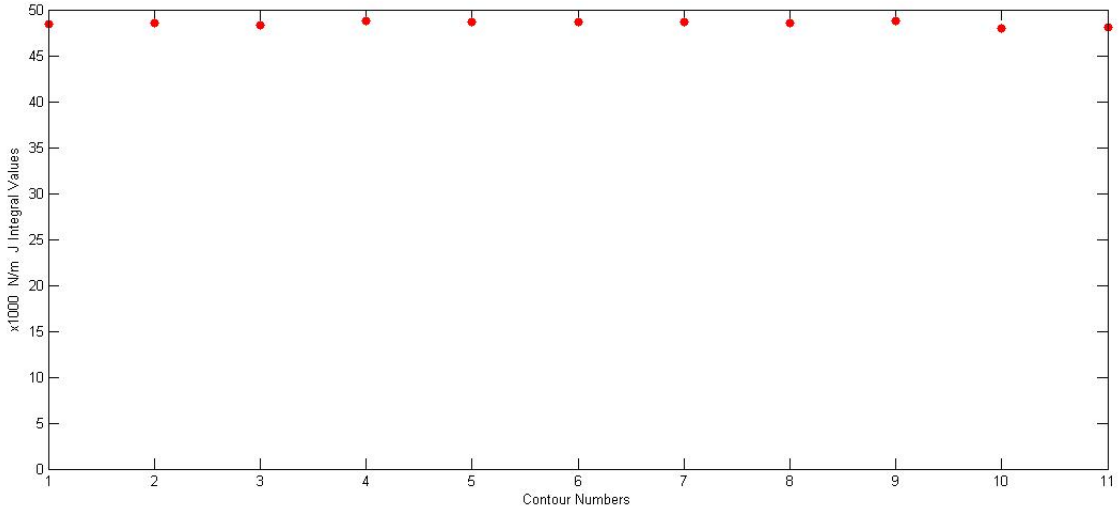

Figure 2.17. J integral values for $\sigma^{\infty} = 50$MPa, $\frac{a}{B} = 0.5$ in fully austenite region.

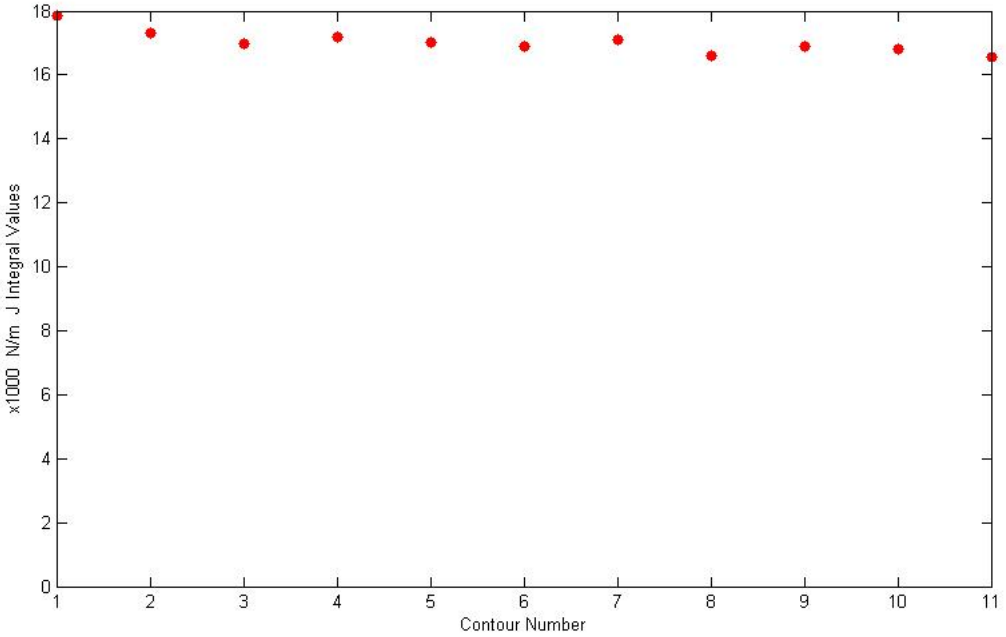

Figure 2.18. J integral values for $\sigma^{\infty} = 30\text{MPa}$, $\frac{a}{B} = 0.5$ in fully martensite region.

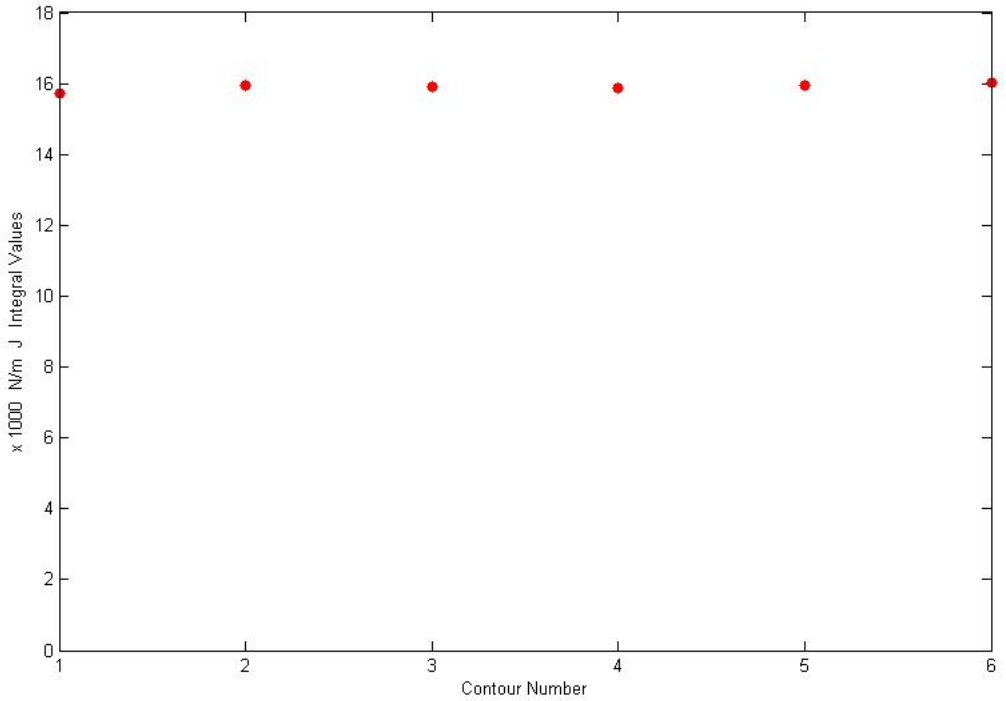

Figure 2.19. J integral values for $\sigma^{\infty} = 30\text{MPa}$, $\frac{a}{B} = 0.5$ in fully austenite region.

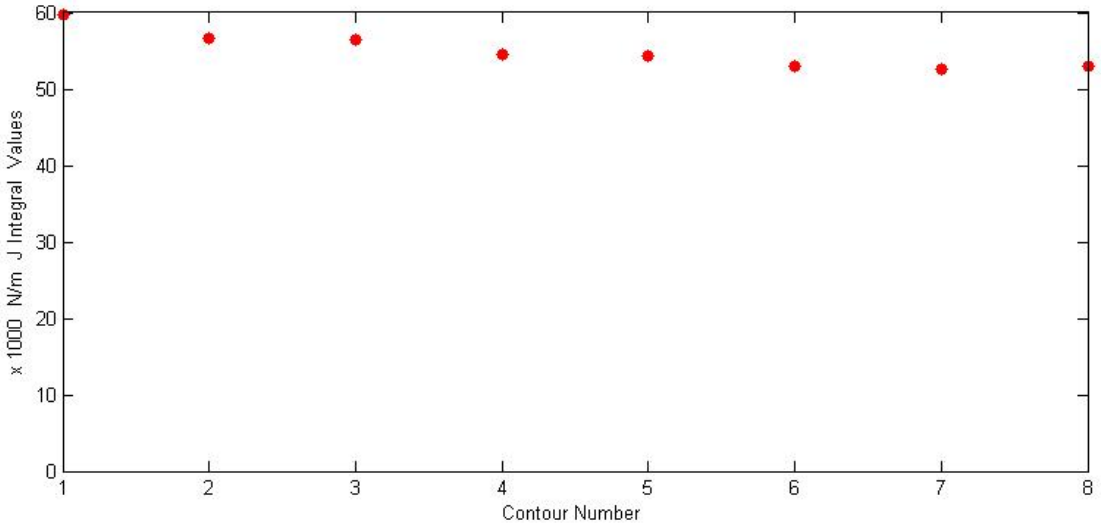

Figure 2.20. J integral values for refined mesh model $\sigma^{\infty} = 50$MPa, $\frac{a}{B} = 0.5$ in fully martensite region.

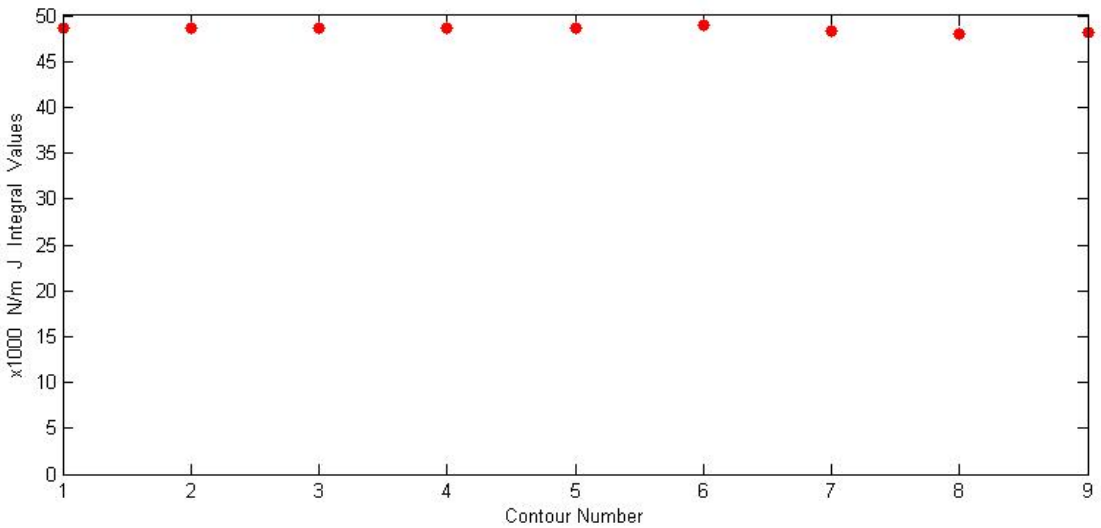

Figure 2.21. J integral values for refined mesh model $\sigma^{\infty} = 50$MPa, $\frac{a}{B} = 0.5$ in fully austenite region.

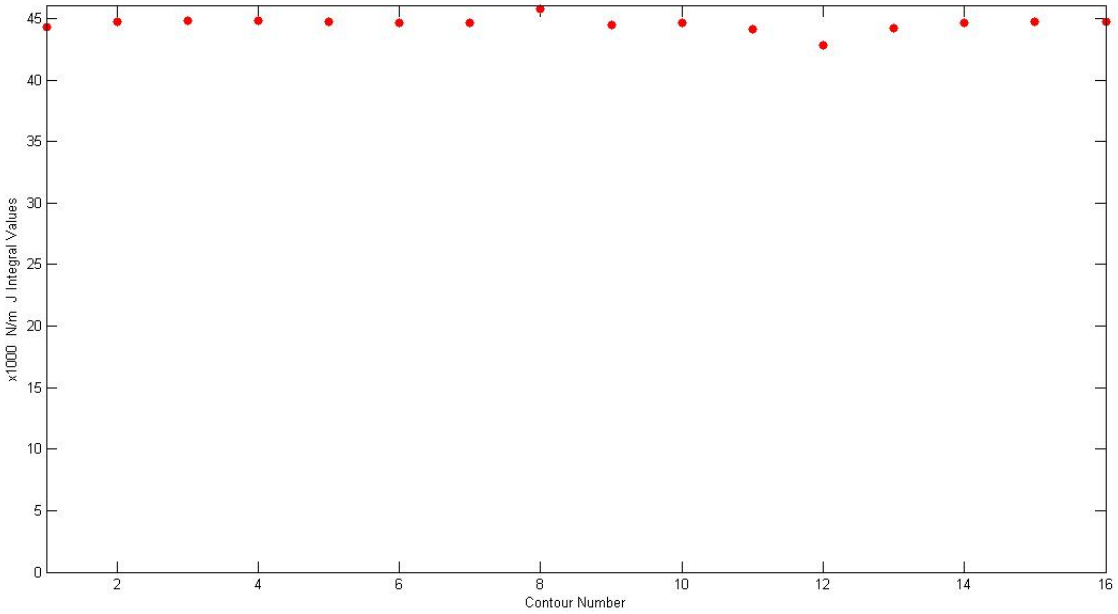

Figure 2.22. J integral values in fully martensite assigned zone for $\sigma^{\infty} = 50$MPa, $\frac{a}{B} = 0.5$.

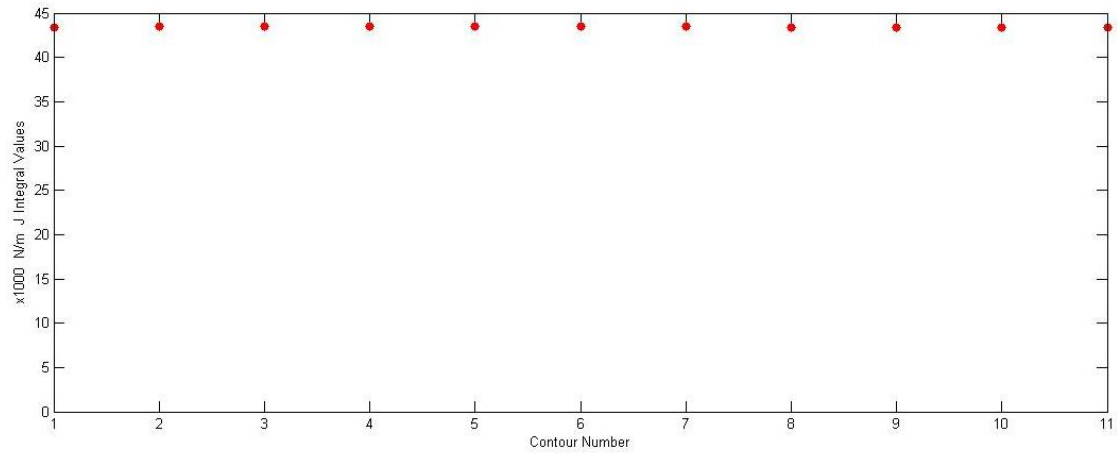

Figure 2.23. J integral values in fully austenite assigned zone for $\sigma^{\infty} = 50$MPa, $\frac{a}{B} = 0.5$.

As can be seen in Figures 2.16 – 2.21 J integral is slowly decreasing in fully martensite zone. ABAQUS inherent J integral algorithm also gives varying values in fully martensite zone. The values decrease as getting further away from crack tip. In

fully austenite zone both ABAQUS and explicit calculations indicate that J integral is constant. The difference in values between two zones result from the transformation phenomenon. In reference [49], the J integral values are calculated by ABAQUS and constant austenite zone values are confirmed.

J integral is shown to be path independent in fully austenite region but path dependent in fully martensite zone. If the material studied were linear elastic, austenitic, isotropic, homogeneous; J integral value would be 41515 $\frac{N}{m}$ and 14463 $\frac{N}{m}$ for $\sigma^{\infty} =$ 50 MPa and $\sigma^{\infty} = 30$ MPa respectively. Hence, J integral values increase due to transformation. The reason behind can be seen if J integral for general materials is written.

$$J = \int_C (w\delta_{1j} - \sigma_{ij}u_{i,1})n_j dC \tag{2.10}$$

The increase of work done by the external tractions in transforming materials (The area under monotonic tensile curve is larger for shape memory alloys than linear elastic materials in order to visualize) causes J integral values increase. For this reason stress work increases and J integral values are larger than austenite linear elastic analogues . However, this work does not directly increase elastic stress. Hence, it does not cause stress intensity factor increase. In fact, stress intensity factor decreases because of transformation strain and chemical free energy.

2.2. Determination of Stress Intensity Factor from J Integral

J integral is an important parameter in order to determine crack tip stress magnitude for a specific loading configuration . In LEFM theory, J integral is contour independent. Utilizing this property, J integral is easily evaluated at an outer contour where stress field is not disturbed by presence of crack. J integral value is related to

stress intensity factor at the crack tip as follows:

$$J = \frac{K_I^2}{E} \tag{2.11}$$

This relation holds for every contour from lower crack face to upper crack face in elastic materials . However, in shape memory alloys J values are contour dependent as shown above. For this reason, J value and elastic modulus value are taken at the crack tip. Then relation between stress intensity factor and J integral at the tip, J_{tip}, can be written as the following expression by taking E_{tip} equal to $E_{martensite} = 28$ GPa.

$$J_{tip} = \frac{K^{tip2}}{E_{tip}} \tag{2.12}$$

The following table shows far field loading σ^{∞}, crack size ratio with respect to plate width a/B, J integral values at the first contour around the crack tip J_{tip}, J integral value in fully austenite region J^{∞}, stress intensity factor K^{tip} in fully martensite zone at the crack tip, stress intensity factor sensed in the fully austenite zone K_I and stress intensity factor for linear elastic material having same far field load and a/B ratio K^{∞}.

Table 2.14. Table showing fracture parameters near the crack tip martensite zone and far field austenite zone

σ^{∞} MPa	a/B	J_{tip} $\frac{N}{m}$	J^{∞} $\frac{N}{m}$	K^{tip} MPa$\sqrt{m}$	K_I MPa$\sqrt{m}$	K^{∞} MPa$\sqrt{m}$
50	0.5	54017.2	48457.2	38.9	36.8	55.8
30	0.5	17862.8	15737.8	22.3	21	33.5

The table above clearly shows that stress intensity factor magnitude decreases with respect to linear elastic material under the same loading conditions and geometry effects. This decrease in stress intensity factor value can be named as transformation toughening. However, whether relation between J^{tip} and K^{tip} is valid or not is de-

batable. Analytical, full field boundary value problem solution is not available, thus a direct analytical relation between J integral value and stress intensity factor magnitude is not known.

2.3. Stress Intensity Factor Calculation by Tri-Linear Model

To model shape memory alloy constitutive behaviors, plasticity type arguments and approaches are used . Some approaches to model pseudoelastic behaviour are inspired from deformation plasticity. The tri-linear model proposed by Maletta *et al.* recently [50-52] based on deformation plasticity in order to calculate stress intensity factor K_{Ie} at the crack tip after transformation. They adopted effective crack size approach and tried to find an effective stress intensity factor K_{Ie}. Their model is restricted to $\theta = 0$. They found σ^M (stress component in y direction on y plane at the boundary of the martensite zone) and boundaries for fully martensite and austenite zones at $\theta = 0$ (r^M and r^A) as the following:

$$\sigma^M = \frac{1}{2(1-\nu) + ((\alpha^*)^{-}1 - 1)} \left[2(1-\nu) \frac{K_{Ie}}{\sqrt{2\pi r}} + ((\alpha^*)^{-1} - 1)\sigma^{tr} - \epsilon_L E_A \right] \tag{2.13}$$

$$r_M = \frac{1}{2\pi} \left(\frac{2(1-\nu)K_{Ie}}{2(1-\nu)(\sigma^{tr} + b_M(T - T^o)) + \epsilon_L E_A} \right)^2 \tag{2.14}$$

$$r^A = 2r^* - \frac{1}{\pi} \left(\frac{K_{Ie}}{\sigma^{tr}} \right)^2 \frac{2(1-\nu)^2}{(2(1-\nu) + ((\alpha^*)^{-1} - 1))(2(1-\nu) + \frac{\epsilon_L E_A}{\sigma^{tr}})} \tag{2.15}$$

$$r^* = \frac{1}{2\pi} \left(\frac{K_I}{\sigma^{tr}} \right)^2 \tag{2.16}$$

$$\Delta r = r^A - r^* \tag{2.17}$$

$$a_e = a + \Delta r \tag{2.18}$$

$$K_{Ie} = \sigma^{\infty}\sqrt{\pi a_e} \tag{2.19}$$

In these equations, α^* is the ratio between elastic moduli of martensite and austenite phases, ϵ_L and σ^{tr} are transformation strain and constant transformation stress observed during monotonic tensile loading respectively, T and T^o are medium temperature and reference temperature respectively and b_M is material constant. K_I is obtained from linear elastic fracture mechanics solution by using far field applied tensile stress σ^{∞}. a and a_e are crack length and effective crack length respectively. These seven unknowns are solved by seven equations listed above.

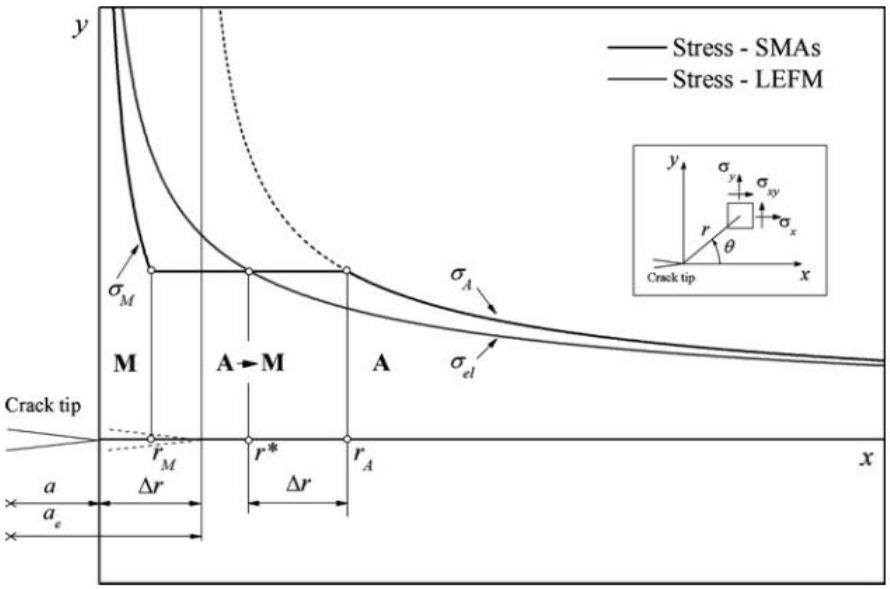

Figure 2.24. Schematic depiction of the stress distribution and phase transformation near the crack tip [52].

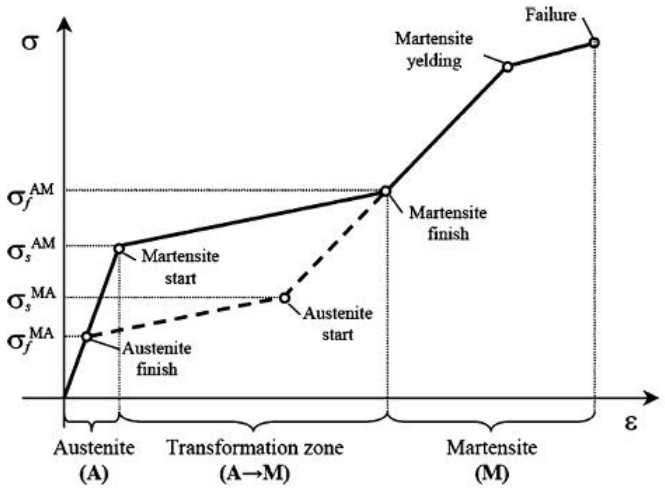

Figure 2.25. Stress-strain relation for tri-linear shape memory alloy material [50].

2.3.1. Proportional Loading Test by Principal Axis and Budiansky Methods

A significant detail about this deformation plasticity based approach is that it does solve the problem by a non-linear elasticity approach rather than an iterative solution schematic based on computational plasticity. First of all, deformation plasticity using proportional loading assumption is valid only in loading. In unloading, the model is not capable of calculating stress and strains correctly. Secondly, the proportions between stress and strain components are assumed to be same in both linear elastic austenite and linear elastic martensite. However, this is debatable in numerical approaches such as Auricchio *et al.*'s finite element model [21-22] since during transformation normality rule may not result in constant ratios between stress and strain tensor components. In that regard, the two methods approach the problem from different directions. Stress, strain and volumetric martensite fraction distributions will be different in these two models.

Whether the deformation plasticity theory utilization is apt or not for a boundary value problem can be checked by Bernard Budiansky's deformation plasticity check criterion [53] and extracting principle directions of stress - strain from finite element analysis for different step increments. Budiansky started the problem solution by two

important postulates of plasticity. These inequalities are:

$$\dot{\sigma_{ij}}\dot{\epsilon_{ij}} \geq 0 \tag{2.20}$$

$$(\sigma_{ij} - \sigma^*_{ij})\dot{\epsilon_{ij}} \geq 0 \tag{2.21}$$

where σ_{ij} is current stress state on on yield surface and σ^*_{ij} is any stress state in elastic domain. The dots indicate derivative with respect to time . From these two inequalities following results are derived:

(i) Yield surface is convex.

(ii) For any loading increment $\dot{\sigma_{ij}}$, $\dot{\epsilon^p_{ij}}$ must be exterior normal to the yield surface.

(iii) If S (yield surface defined in σ_{ij} space) is not smooth at σ_{ij} which means there is no unique normal at that point, $\dot{\epsilon^p_{ij}}$ must point toward the region bounded by the cone of normals to S at at σ_{ij} The following figure illustrates case (iii). Although propor-

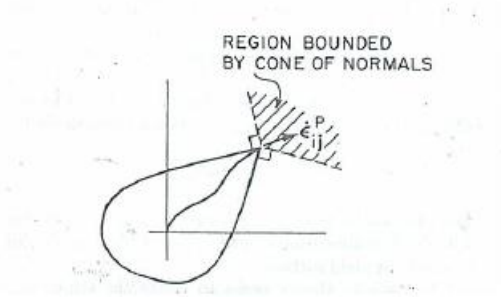

Figure 2.26. Direction of $\dot{\epsilon^p_{ij}}$ at a corner of yield surface [53].

tional loading implies constant principal directions of deviatoric stress during loading (that is disregarding hydrostatic components since yield surface does only depend on deviatoric components in classical plasticity theory), some small deviations from this can still be acccepted as proportional in the small neighborhood of loading direction in stress space. Budiansky imposed two conditions that need to be fulfilled in order to use proportional loading arguments in a problem. These are summarized briefly as the following equations and illustrated by the subsequent two figures geometrically.

(i) $\alpha \leq \beta$

$$\alpha = \cos^{-1} \frac{s_{ij}\dot{s_{ij}}}{\sqrt{s_{kl}s_{kl}}\sqrt{\dot{s_{mn}}\dot{s_{mn}}}} \tag{2.22}$$

α is the angle between central axis of cone formed by non smooth yield surface exterior normals and deviatoric stress increment, β is the semivertex angle of the cone.

(ii) $\delta + \beta \leq \frac{\pi}{2}$

$$\delta = \cos^{-1} \frac{s_{ij}\dot{\epsilon^p_{ij}}}{\sqrt{s_{kl}s_{kl}}\sqrt{\dot{\epsilon^p_{mn}}\dot{\epsilon^p_{mn}}}} \tag{2.23}$$

δ is the angle between central axis of cone and plastic strain increment.

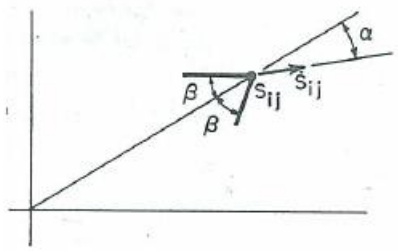

Figure 2.27. Illustration of β and the angle between s_{ij} and $\dot{s_{ij}}$ [53].

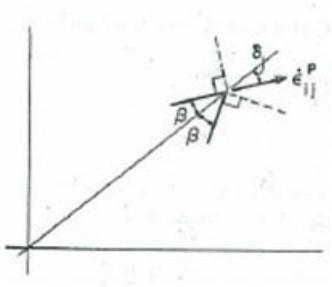

Figure 2.28. Angle between $\dot{\epsilon}^p_{ij}$ and s_{ij} [53].

Checking these two conditions enables one to determine whether the loading can be accepted as proportional loading or not. In order to check these conditions , Auricchio *et al.*'s model [21-22] results were used. In this model, when the material parameters in the previous chapter is used, the transformation surface only depends on deviatoric stress components. Hence, Budiansky's approach [53] is applicable.

Firstly standart principal direction coincidence check was carried out. An edge cracked thin plate under plane stress Mode I loading with $\frac{a}{B} = \frac{50mm}{100mm}$ was analysed with an applied far field loading of $\sigma^{\infty} = 20$ MPa. A material point that is at an angle of $\frac{\pi}{4}$ radians with respect to x axis of the finite element model used in the previous chapter and 0.3 mm away radially from the crack tip, in fully martensite zone was taken at first. During each step increment, the material point chosen was monitored whether ratios of principle values of deviatoric stress had changed or not . The following figure shows the values of these ratios in deviatoric stress space formed by s_{11}, s_{22}, s_{12}.

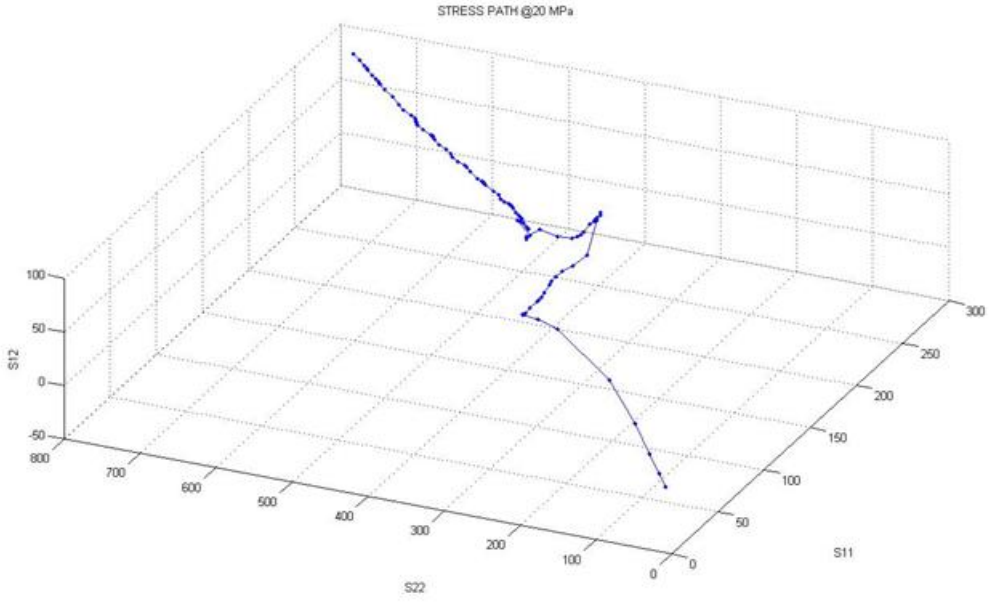

Figure 2.29. For $\sigma^{\infty} = 20MPa$ and $\frac{a}{B} = \frac{50}{100}$, the stress path traversed in deviatoric stress space.

As one can see Budiansky's restrictions are violated and proportional loading condition is not valid at this point in the fully transformed martensite zone near the crack tip. Another material point was selected in the same model in order to confirm the result of nonproportional loading aforementioned. This time the initial radial coordinate of the point is $r = 0.03$ and at angle of $\frac{\pi}{4}$ radians with respect to x axis. The resultant path can be viewed in the next figure.

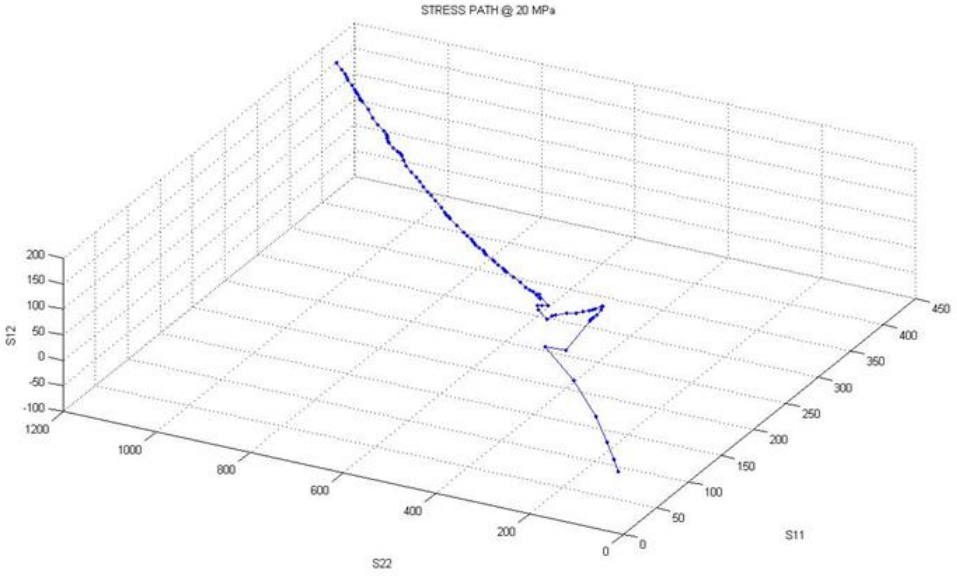

Figure 2.30. For $\sigma^{\infty} = 20$ MPa and $\frac{a}{B} = \frac{50}{100}$, the stress path traversed in deviatoric stress space.

The second test also confirmed that the loading is nonproportional. The reason is transformation strain evaluated by normality rule. Hence using proportional loading arguments with deformation plasticity as Maletta *et al.* [50-52] gives different results compared to Auricchio *et al.*'s iterative finite element solution methodology [21-22].

3. DETERMINATION OF FRACTURE PARAMETERS BASED ON MICROMECHANICAL APPROACHES

3.1. Eshelby Approach for Transforming Inhomogeneity

In micromechanical approach of shape memory alloy modelling, Eshelby's inclusion method is used [27,43]. For a volume where transformation takes place inside infinite matrix under prescribed loading, Eshelby showed that the isotropic inhomogeneity (it has different elastic constants from surrounding matrix) can be replaced by a homogeneous isotropic inclusion that has the same elastic constants as the matrix by including an additional eigenstrain (stress free transformation strain) inside. For this substitution, there are two restrictions to be fulfilled : the traction and displacement fields must be matched across the interface of inclusion (inclusion and matrix have the same elastic constants). Sufficent conditions for these are equivalence of elastic stress field and total strain field between two configurations. Stress inside inhomogeneity can be written as the following expression.

$$\sigma_{ij}^{M} = C_{ijkl}^{M}(\epsilon_{kl}^{a} + \epsilon_{kl}^{*} - \epsilon_{kl}^{tr}) \tag{3.1}$$

where C_{ijkl}^{M}, ϵ_{kl}^{a}, ϵ_{kl}^{*}, ϵ_{kl}^{tr} are elastic stiffness tensor for martensite inhomogeneity, uniform far field applied strain, additional strain caused due to restriction of stress free transformation strain inside inhomogeneity by the surrounding matrix and stress free transformation strain (eigenstrain) respectively.

Stress inside inclusion has to have the same stress field inside but expressed in a slightly different way:

$$\sigma_{ij}^{M} = C_{ijkl}^{A}(\epsilon_{kl}^{a} + \epsilon_{kl}^{*} - \epsilon_{kl}^{tr} - \epsilon_{kl}^{**}) \tag{3.2}$$

where C^A_{ijkl}, ϵ^*_{kl}, ϵ^{**}_{kl} are elastic stiffness tensor for austenite matrix, additional strain caused due to restriction of stress free transformation strain inside inhomogeneity by the surrounding matrix, additional eigenstrain in inclusion (added in order to sustain the same stress field as martensite inhomogeneity) respectively. Total strain inside inhomogeneity:

$$\epsilon^{inhomogeneity}_{kl} = \epsilon^A_{kl} + \epsilon^*_{kl} \tag{3.3}$$

Total strain inside inclusion:

$$\epsilon^{inclusion}_{kl} = \epsilon^A_{kl} + \epsilon^*_{kl} \tag{3.4}$$

Also, it should be kept in mind that if ϵ^{tr}_{kl} is uniform inside inhomogeneity then $\epsilon^{tr}_{kl} + \epsilon^{**}_{kl}$ is also uniform inside inclusion as long as it is ellipsoid in shape. Then utilizing the equivalency of stress field in inhomogeneity and inclusion, following expression is obtained.

$$C^M_{ijkl}(\epsilon^a_{kl} + \epsilon^*_{kl} - \epsilon^{tr}_{kl}) = C^A_{ijkl}(\epsilon^a_{kl} + \epsilon^*_{kl} - \epsilon^{tr}_{kl} - \epsilon^{**}_{kl}) \tag{3.5}$$

Strain disturbance in the ellipsoid inclusion or inhomogeneity due to restriction by the surrounding medium can be written as:

$$\epsilon^*_{kl} = S_{klmn}(\epsilon^{tr}_{mn} + \epsilon^{**}_{mn}) \tag{3.6}$$

where S_{klmn} is called Eshelby's Tensor (4^{th} order tensor and constant for constant ϵ^{tr}_{kl})

As a result in explicit form the equivalence of stress field inside transformed zone

can be written as :

$$C^M_{ijkl}(\epsilon^a_{kl} + S_{klmn}(\epsilon^{tr}_{mn} + \epsilon^{**}_{mn}) - \epsilon^{tr}_{kl}) = C^A_{ijkl}(\epsilon^a_{kl} + S_{klmn}(\epsilon^{tr}_{mn} + \epsilon^{**}_{mn}) - \epsilon^{tr}_{kl} - \epsilon^{**}_{kl}) \quad (3.7)$$

solving for ϵ^{**} tensor:

$$\begin{aligned} \epsilon^{**}_{ab} = &\left[(C^M_{ijrs} - C^A_{ijrs})S_{rsab} + C_{ijrs}\delta_{ra}\delta_{sb}\right]^{-1} \\ &\left[(C^A_{ijkl} - C^M_{ijkl})\epsilon^a_{kl} + \left[(C^M_{ijkl} - C^A_{ijkl})\delta_{km}\delta_{nl} + (C^A_{ijkl} - C^M_{ijkl})S_{klmn}\right]\epsilon^{tr}_{mn}\right] \end{aligned} \quad (3.8)$$

Determination of stress free transformation strain is critical in this formulation. This can be found using the procedures introduced by Wechsler *et al.* [54], Khachaturyan [55] and Bhattacharya [5]. Stress intensity factor evaluation methods inspired from transforming inhomogeneity approach are discussed in the following sections.

3.2. Weight Function Approach to Determine Stress Intensity Factor

Quantifying stress intensity factor change due to stress induced transformation has attracted interest from reseachers in the recent years. Yi and Gao [24] extracted eigenstrain from finite element results based on constitutive model of Sun *et al.* [25-26]. The transformation strains are used in weight function approach of Rice [29]. This results stress intensity factor change due to martensitic transformation.

A similar analysis under plane stress using Auricchio *et al.*'s constitutive model [21-22]. Material properties used in the finite element calculations are listed in the following table.

Table 3.1. Material data used in ABAQUS model.

Austenite Modulus	75 GPa
Martensite Modulus	28 GPa
Transformation Strain	4%
Martensite Transformation Start Stress ($295K$)	400 MPa
Martensite Transformation Finish Stress ($295K$)	400.5 MPa
Austenite Transformation Start Stress ($295K$)	300.5MPa
Austenite Transformation Finish Stress ($295K$)	300 MPa
Transformation Stress Change w.r.t Temperature	$5.4\frac{MPa}{K}$
Martensite Transformation Start Stress under Compression	400 MPa
ν (Poisson Ratio of Martensite and Austenite)	0.33

In this analysis CPS8 element, as in the previous chapter, was selected. After obtaining results, transformation strain components were extracted on fully transformed martensite region. The inclusion shape was taken as spherical. Eshelby tensor for spherical inclusion is given in Voigt representation as:

$$[S_{klmn}] = \frac{1}{15(1-\nu)} \begin{bmatrix} 7-5\nu & 5\nu-1 & 5\nu-1 & 0 & 0 & 0 \\ 5\nu-1 & 7-5\nu & 5\nu-1 & 0 & 0 & 0 \\ 5\nu-1 & 5\nu-1 & 7-5\nu & 0 & 0 & 0 \\ 0 & 0 & 0 & 2(4-5\nu) & 0 & 0 \\ 0 & 0 & 0 & 0 & 2(4-5\nu) & 0 \\ 0 & 0 & 0 & 0 & 0 & 2(4-5\nu) \end{bmatrix}$$

After extracting transformation strain from finite element analysis results and determining additional strain due to constraints from surrounding medium, stress weight function "h" proposed by Rice [29] was used for plane stress. The stress weight func-

tions for 2-D is given as:

$$h_1^1 = \frac{E_A}{2K_I^1}\frac{\partial u_x^{(1)}}{\partial a} \tag{3.9}$$

$$h_2^1 = \frac{E_A}{2K_I^1}\frac{\partial u_y^{(1)}}{\partial a} \tag{3.10}$$

where superscripts 1 indicate that the pertinent quantity belongs to configuration 1 which is any symmetrical linear elastic case where solutions are known for K_I, u_x, u_y under plane stress conditions. Then since from linear elastic solution for Mode I displacement field [8]:

$$u_x = \frac{K_I^{(1)}(1+\nu)}{E_A}\sqrt{\frac{r}{2\pi}}\cos\frac{\theta}{2}\left(\frac{3-\nu}{1+\nu} - 1 + 2sin^2\frac{\theta}{2}\right) \tag{3.11}$$

$$u_y = \frac{K_I^{(1)}(1+\nu)}{E_A}\sqrt{\frac{r}{2\pi}}\sin\frac{\theta}{2}\left(\frac{3-\nu}{1+\nu} + 1 - 2cos^2\frac{\theta}{2}\right) \tag{3.12}$$

and from linear elastic fracture mechanics:

$$K_I^{(1)} = F\sigma^{\infty}\sqrt{\pi a} \tag{3.13}$$

Weight functions $h^{(1)} = [h_1^{(1)}; h_2^{(1)}]$ are universal functions for any given geometry and compositions according to Rice [29]. These are found as such for plane stress Mode I configuration:

$$h_1^{(1)} = \frac{1+\nu}{4\sqrt{2\pi r}}\cos\frac{\theta}{2}\left(1 - \frac{3-\nu}{1+\nu} - 2\sin^2\frac{\theta}{2} + 2\sin^2\theta\right) \tag{3.14}$$

$$h_2^{(1)} = \frac{1+\nu}{4\sqrt{2\pi r}}sin\frac{\theta}{2}\left(\frac{3-\nu}{1+\nu} + 1 - 2cos^2\frac{\theta}{2} + 2sin^2\theta\right) \tag{3.15}$$

$$\tag{3.16}$$

Second configuration was taken as the configuration where transformed zone was kept in its undeformed shape due to tractions applied on the surface as seen in Figure 1.8. Stress intensity factor of second configuration can be found as the following:

$$K_I^{(2)} = \int_\Gamma T_i^{(2)} h_i^{(1)} d\Gamma \tag{3.17}$$

where T_i^2 is surface traction component pertinent to second configuration and h_i^1 is weight function for first configuration which can be chosen as Mode I geometry subjected to uniform far field applied tensile stress σ^∞. If this outer boundary field is same for both cases then the only difference shows up due to transformation is transformation induced tractions on the transformation finish zone boundary Γ. Calling $K_I^{(2)} \equiv K^{tip}$ and $K_I^{(1)} \equiv K^\infty$

$$\Delta K = \int_\Gamma n_i C_{ijkl}^A (S_{klmn}(\epsilon_{mn}^{**} + \epsilon_{mn}^{tr}) - \epsilon_{mn}^{tr} - \epsilon_{mn}^{**}) h_j^{(1)} d\Gamma \tag{3.18}$$

Resultant crack tip stress intensity factor is obtained by:

$$K^{tip} = K^\infty - \Delta K^{tip} \tag{3.19}$$

K^∞ is linear elastic fracture mechanics solution obtained for austenite phase neglecting transformation under same outer far field stress field σ^∞. In this equation negative sign implies that if $\epsilon_{ij}^{**} + \epsilon_{ij}^{tr}$ taken to be positive then traction needed to fit the inclusion back, without any deformation in the surrounding medium, will be negative (inward direction). In this regard, traction applied on initial geometry will be compressive. This results toughening due to transformation.

In the following figures, dotted points indicate stress values found by finite element analysis, red line shows fit of these data to asymptotic LEFM equation, blue line shows asymptotic LEFM equation used by K^{tip} obtained from aforementioned procedure. Lastly black line corresponds to classical linear elastic fracture mechanics solution without any transformation. The difference between the two approaches may result

from the fact that Auricchio *et al.*'s constitutive model [21-22] is plasticity based. It does not consider any micromechanical phenomena. However, Sun *et al.*'s constitutive model [25-26] based on free energy expressions including Mori-Tanaka self-consistent averaging [43] and Eshelby [27] inclusion method taking geometry of inclusions as spherical.

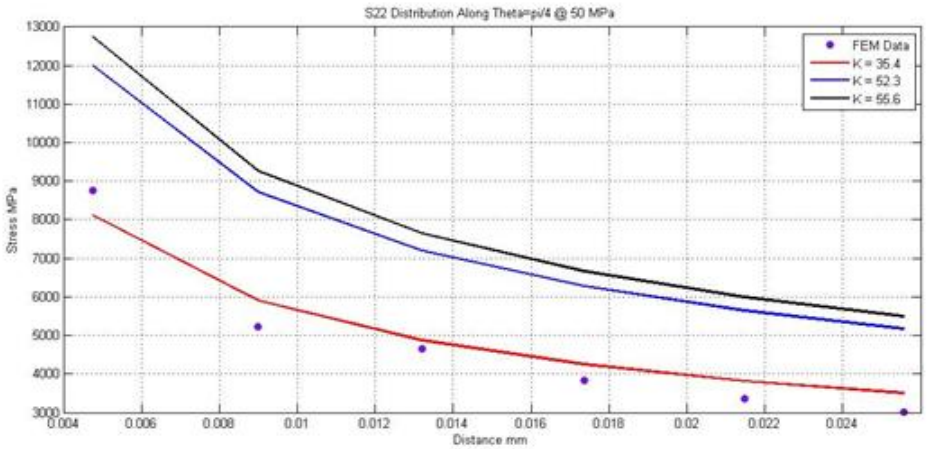

Figure 3.1. Comparisons of stress distribution near the crack tip in fully transformed martensite zone for ABAQUS finite element analysis, linear elastic fracture mechanics solution and inclusion method for $\sigma^{\infty} = 50$ MPa at $\theta = \frac{\pi}{4}$ radians.

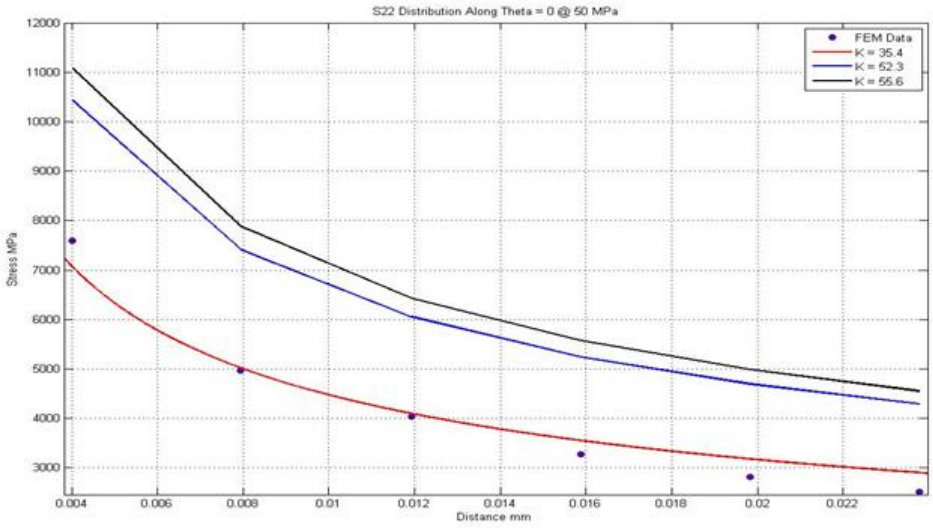

Figure 3.2. Comparisons of stress distribution near the crack tip in fully transformed martensite zone for ABAQUS finite element analysis, linear elastic fracture mechanics solution and inclusion method for $\sigma^{\infty} = 50$ MPa at $\theta = 0$ radians.

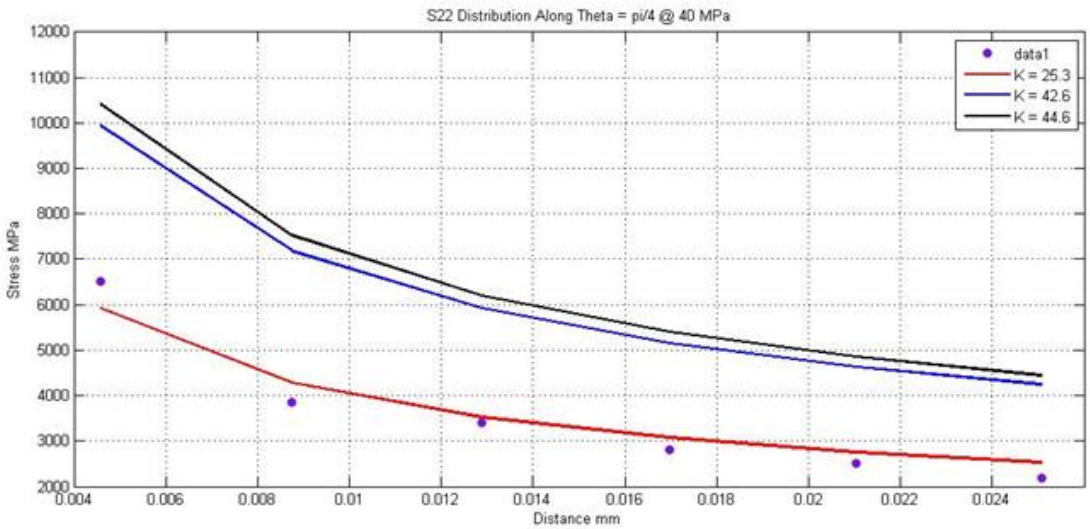

Figure 3.3. Comparisons of stress distribution near the crack tip in fully transformed martensite zone for ABAQUS finite element analysis, linear elastic fracture mechanics solution and inclusion method for $\sigma^{\infty} = 40$MPa at $\theta = \frac{\pi}{4}$ radians.

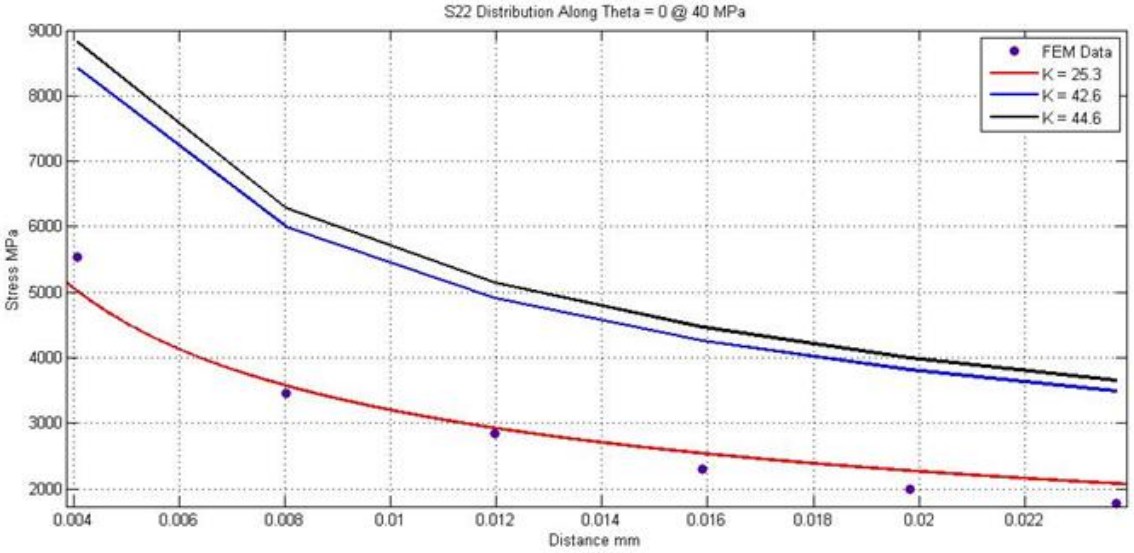

Figure 3.4. Comparisons of stress distribution near the crack tip in fully transformed martensite zone for ABAQUS finite element analysis, linear elastic fracture mechanics solution and inclusion method for $\sigma^{\infty} = 40$ MPa at $\theta = 0$ radians.

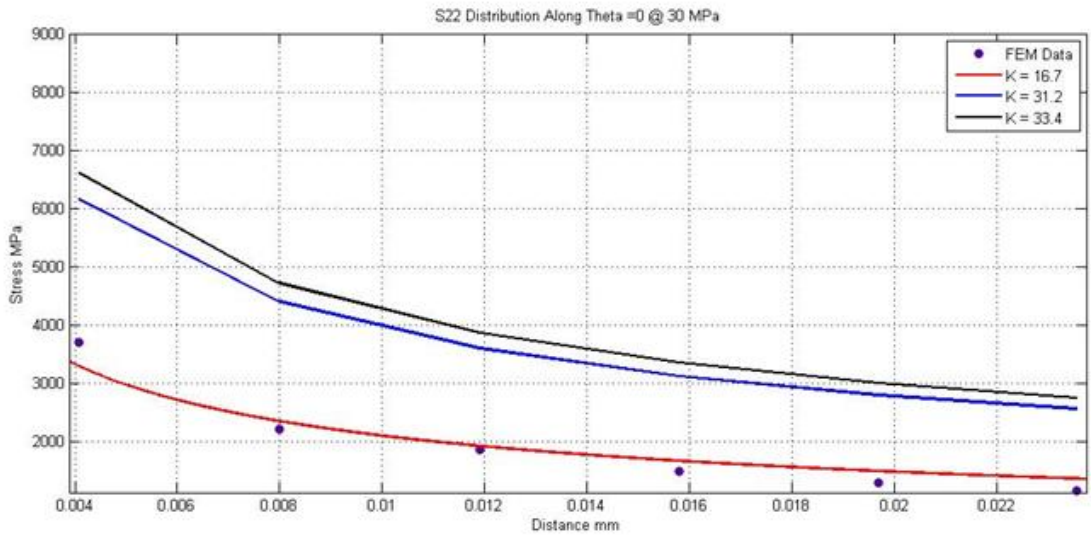

Figure 3.5. Comparisons of stress distribution near the crack tip in fully transformed martensite zone for ABAQUS finite element analysis, linear elastic fracture mechanics solution and inclusion method for $\sigma^{\infty} = 30$ MPa at $\theta = 0$ radians.

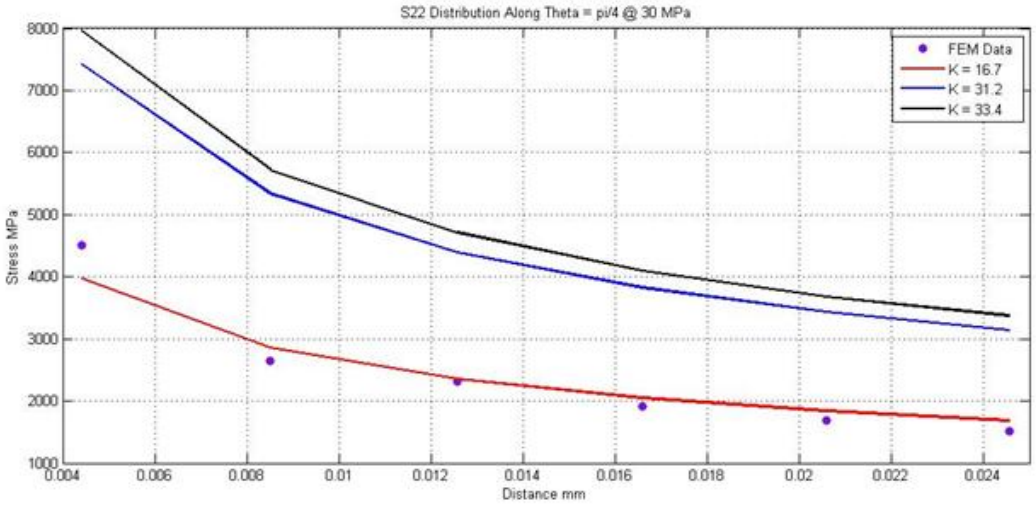

Figure 3.6. Comparisons of stress distribution near the crack tip in fully transformed martensite zone for ABAQUS finite element analysis, linear elastic fracture mechanics solution and inclusion method for $\sigma^{\infty} = 30$ MPa at $\theta = \frac{\pi}{4}$ radians.

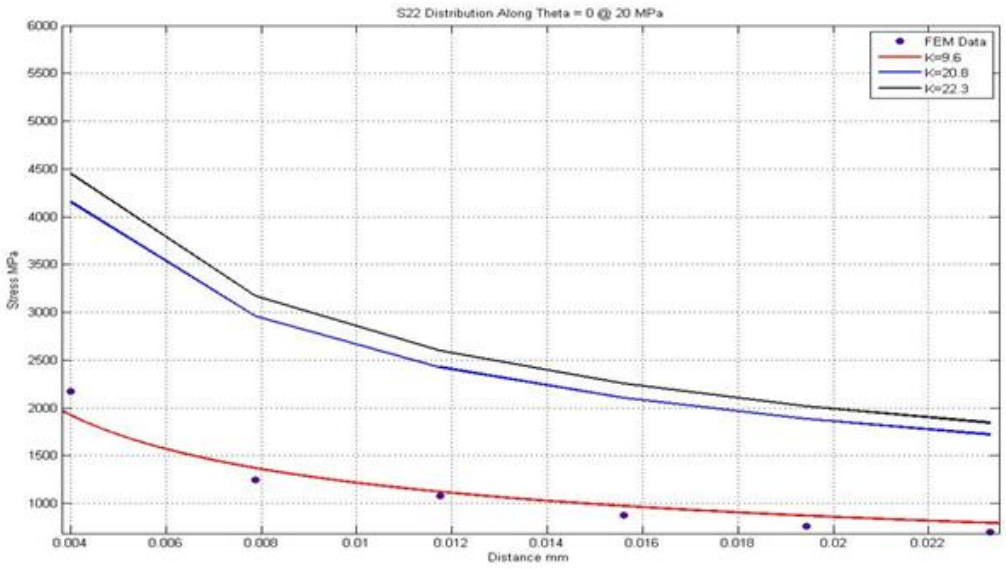

Figure 3.7. Comparisons of stress distribution near the crack tip in fully transformed martensite zone for ABAQUS finite element analysis, linear elastic fracture mechanics solution and inclusion method for $\sigma^{\infty} = 20$ MPa at $\theta = 0$ radians.

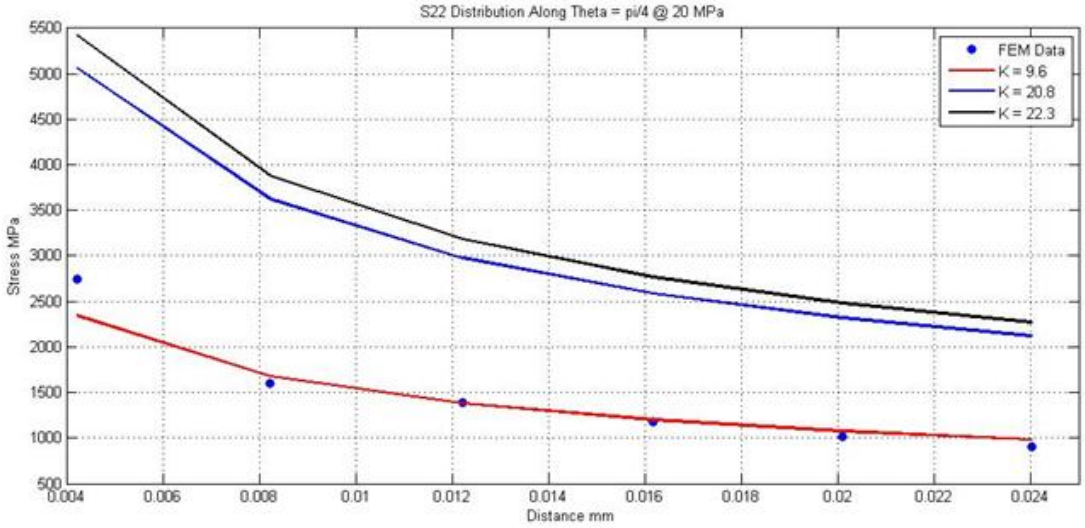

Figure 3.8. Comparisons of stress distribution near the crack tip in fully transformed martensite zone for ABAQUS finite element analysis, linear elastic fracture mechanics solution and inclusion method for $\sigma^{\infty} = 20$ MPa at $\theta = \frac{\pi}{4}$ radians.

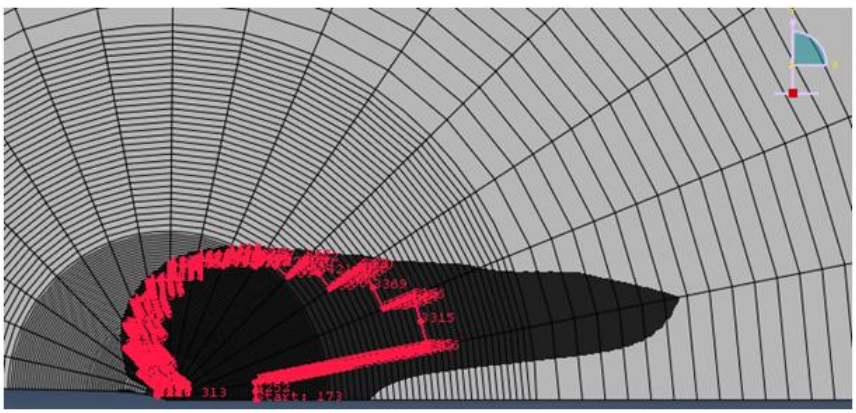

Figure 3.9. Path for $\sigma^{\infty} = 50$ MPa enclosing fully martensite zone at the crack tip is shown above. The dark regions indicate where volumetric martensite fraction is bigger than 0.

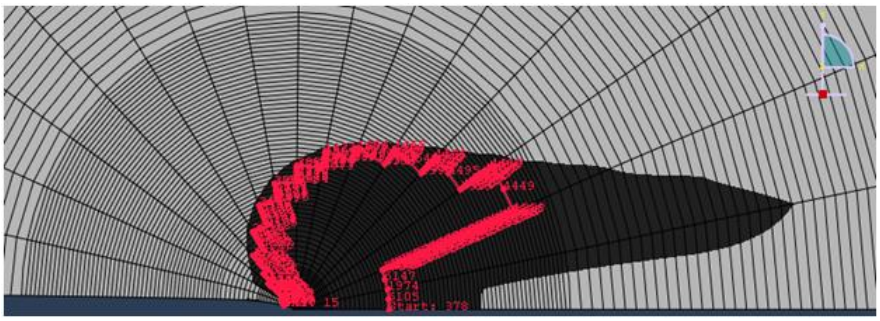

Figure 3.10. Path enclosing fully transformed martensite region at 40MPa far field loading.

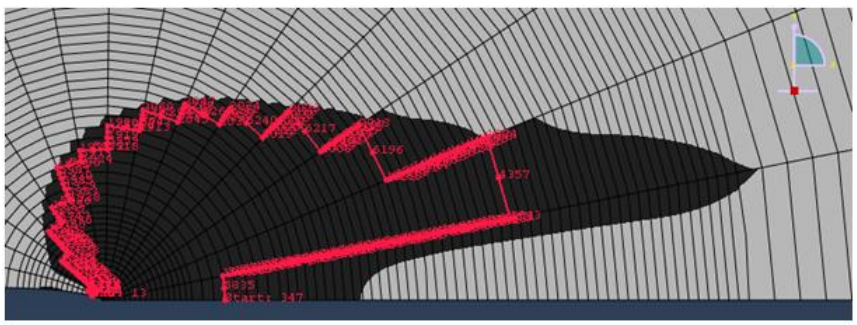

Figure 3.11. Path enclosing around fully transformed martensite region for 30 MPa far field stress.

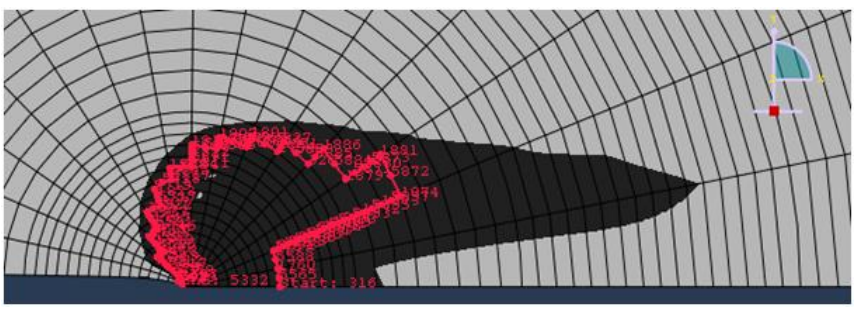

Figure 3.12. Path encloses fully transformed region for 20 MPa far field stress applied configuration.

3.3. Evaluation of Stress Intensity Factor Change by Eigenstrains

In order to calculate crack tip stress field interaction with stress free transformation strain, stress free transformation should be evaluated. Wechsler *et al.* [54] and Khachaturyan [55] gave detailed explanations to calculate transformation strain from lattice parameters using invariant plane approach. The stress free transformation strain will not be only one value but it will differ according to chosen variants which depend on the stress and strain states. However, the stress field is also affected by the selection of variant. Thus, it results a coupled problem for a crystal.

Firstly, stress free transformation strains of different variants will be determined for single crystal NiTi alloy (49.8% Ni) from lattice parameters [56]. Then in order to have an idea about the polycrystal structure , different grain orientation distributions will be chosen. The variants selected near crack tip , will be determined from asymptotic linear elastic fracture mechanics stress field. Lastly, Hutchinson's formula [57,58] for stress intensity factor change due to a point defect undergoing transformation under Mode I will be used to demonstrate the effect of phase transformation on stress intensity factor. The evaluations do not take reorientation (detwinning) of martensite phase into account since it is very complicated due to coupled nature of phenomenon.

For each variant, transformation strain was calculated by determining the invariant plane and shear direction on this plane. Then traditional Schmid factor tensor [59] used in classical plasticity as the following:

$$V_{ij} = \frac{1}{2}(n_i \Lambda_j + n_j \Lambda_i) \tag{3.20}$$

where n_i and Λ_i are component of habit plane normal and shear vector component on this plane respectively.

This tensor is multiplied by γ which is two times the tensorial strain component on invariant plane in shear direction and added to the tensor formed by multiplying dyadic product $(n_i n_j)$ with ψ which is the strain component on invariant plane in

normal direction. This can be written as below.

$$\epsilon_{ij}^{tr} = V_{ij}\gamma + \psi(n_i n_j) \tag{3.21}$$

During determination procedure of average transformation strain, as the first case, equal volume fraction of each martensite variant was assumed. In order to ease the evaluation, crystal coordinate system of each crystal was assumed to coincide with global coordinate system used in macro scale. The following table shows martensite variants, related planes and shear directions on these habit planes with respect to crystal coordinate system for NiTi.

Table 3.2. Variant habit planes and directions [56].

Variants	**Habit planes**	**Shear directions**
1–2	$(0.8889, 0.2152, -0.4044)$	$[-0.4114, 0.7633, -0.4981]$
1–2′	$(0.8889, 0.4044, -0.2152)$	$[-0.4114, 0.4981, -0.7633]$
1′–2	$(-0.8889, 0.4044, -0.2152)$	$[0.4114, 0.4981, -0.7633]$
1′–2′	$(-0.8889, 0.2152, -0.4044)$	$[0.4114, 0.7633, -0.4981]$
2–1	$(0.8889, 0.2152, 0.4044)$	$[-0.4114, 0.7633, 0.4981]$
2–1′	$(0.8889, 0.4044, 0.2152)$	$[-0.4114, 0.4981, 0.7633]$
2′–1	$(-0.8889, 0.4044, 0.2152)$	$[0.4114, 0.4981, 0.7633]$
2′–1′	$(-0.8889, 0.2152, 0.4044)$	$[0.4114, 0.7633, 0.4981]$
3–4	$(0.4044, -0.8889, -0.2152)$	$[0.4981, 0.4114, -0.7633]$
3–4′	$(0.2152, -0.8889, -0.4044)$	$[0.7633, 0.4114, -0.4981]$
3′–4	$(0.2152, 0.8889, -0.4044)$	$[0.7633, -0.4114, -0.4981]$
3′–4′	$(0.4044, 0.8889, -0.2152)$	$[0.4981, -0.4114, -0.4981]$
4–3	$(0.4044, 0.8889, 0.2152)$	$[0.4981, -0.4114, 0.7633]$
4–3′	$(0.2152, 0.8889, 0.4044)$	$[0.7633, -0.4114, 0.4981]$
4′–3	$(0.21520, -0.8889, 0.4044)$	$[0.7633, 0.4114, 0.4981]$
4′–3′	$(0.4044, -0.8889, 0.2152)$	$[0.4981, 0.4114, 0.7633]$
5–6	$(0.2152, -0.4044, 0.8889)$	$[0.7633, -0.4981, -0.4114]$
5–6′	$(0.4044, -0.2152, 0.8889)$	$[0.4981, -0.7633, -0.4114]$
5′–6	$(0.4044, 0.2152, -0.8889)$	$[0.4981, -0.7633, 0.4114]$
5′–6′	$(0.2152, -0.4044, -0.8889)$	$[0.7633, -0.4981, 0.4114]$
6–5	$(0.2152, 0.4044, 0.8889)$	$[0.7633, 0.4981, -0.4114]$
6–5′	$(0.4044, 0.2152, 0.8889)$	$[0.4981, 0.7633, -0.4114]$
6′–5	$(0.4044, 0.2152, -0.8889)$	$[0.4981, 0.7633, 0.4114]$
6′–5′	$(0.2152, 0.4044, -0.8889)$	$[0.7633, 0.4981, 0.4114]$

Given the lattice parameters of both phases, transformation strains of each variant crystal can be found by Khachaturyan's method [55]. According to this method, the transformation strain components for each variant were found by Lu *et al.* [56,60].

For austenite phase (BCC structure) the lattice constant a = 0.3015 nm and for stress induced martensite phase (monoclinic structure) a = 0.2889nm, b = 0.4120 nm, c = 0.4622 nm, $\Omega = 96.8^o$. Using these lattice constants, $\gamma = -0.001174$ and $\psi = 0.13293$ were calculated by Lu *et al.* [56,59]. The transformation strain components can be written by using Equation 3.21 as:

$$\epsilon_{ij}^{tr} = n_i n_j(-0.001174) + V_{ij}(0.13293) \tag{3.22}$$

The stress field at the crack tip is assumed to have LEFM asymptotic distribution as Lambropoulos [58]. As variant selection criterion, maximization of $\sigma_{ij}\epsilon_{ij}^{tr}$ quantity was used. In this expression as long as asymptotic LEFM stress form was accepted, the active variants are not affected. Thus, stress intensity factor value is ineffective in determining active variants. Near the crack tip this condition gives three dominant variants : 24^{th} between $0-60^o$, 20^{th} between 60^o-120^o , 18^{th} for 120^o-180^o (geometry is symmetric between $180^o - 360^o$).

In order to determine the percentages of these variants , shape of fully transformed martensite region must be determined (partial transformation zone neglected). This should be evaluated by a polycrystal yielding criterion proposed for shape memory alloys . Lexcellent *et al.*'s polycrystal shape memory alloy constitutive model [36-39,41] was chosen. The criterion for yielding is given as the following (assuming that the material shows symmetry between compressive and tensile loading so that criterion simplifies to yield criterion of von Mises).

$$\sigma^{eq} = \sqrt{\frac{3}{2} s_{ij} s_{ij}} \tag{3.23}$$

In the equation above σ^{eq} must be equal to martensite finish stress at 295 K. The material parameters used in this section is summarized in the following table.

Table 3.3. Material properties of NiTi used by Lu *et al.*[56] and Lagoudas *et al.* [61].

Eaustenite	30GPa
Emartensite	13GPa
ν	0.33
α^A	11x10$^{-6}\frac{1}{^oC}$
α^M	6.6x10$^{-6}\frac{1}{^oC}$
M^{0s}	23^oC
M^{0f}	5^oC
A^{0s}	29^oC
A^{0f}	51^oC
C^M	$11.3\frac{MPa}{^oC}$
C^A	$4.5\frac{MPa}{^oC}$
σ^{eq}	192.1 MPa

To determine the area, following expression is used where "r_C" stands for fully martensite finish boundary according to the yield criterion.

$$r_C = \left(\frac{(K^{tip})^2}{2\pi(\sigma^{mf})^2}\right)\cos^2\frac{\theta}{2}\left(1+4\nu^2-4\nu+\frac{1}{3}\sin^2\frac{\theta}{2}\right) \tag{3.24}$$

The percentages of the area covered by different variants are not effected by K^{tip} value. Active variant percentages are 24 = 43%, variant 20 = 45.2%, variant 18 = 11.8%. These variant ratios were used as weight coefficents when finding the average transformation strain.

After determining average transformation strain (symbolized as ϵ_{ij}^{tr} in the following equations), constrained strain was found. The medium was assumed as infinite compared to spherical particle size. The transformed zone volumetric martensite fraction (ξ) was accepted as 0.99 which is in agreement with Tanaka's exponential formula [19].

In fully martensite zone depending on isotropy the inclusions were accepted to be distributed randomly. Hence, necessary conditions for Mori-Tanaka's averaging theorem [43] were fulfilled . By this theorem, average internal stress equation can be expressed as the following ("<>" indicates average values):

$$\xi < \sigma_{ij} >_M + (1-\xi) < \sigma_{ij} >_A = 0 \tag{3.25}$$

From Eshelby's inhomogenous inclusion method [27]:

$$\xi C^M_{ijkl}(\epsilon^o_{kl} + S_{klmn}(\epsilon^{tr}_{mn} + \epsilon^{**}_{mn}) - \epsilon^{tr}_{kl}) + (1-\xi)C^A_{ijkl}\epsilon^o_{kl} = 0 \tag{3.26}$$

or in terms of austenite medium properties :

$$\xi C^A_{ijkl}(\epsilon^o_{kl} + S_{klmn}(\epsilon^{**}_{mn} + \epsilon^{tr}_{mn}) - \epsilon^{**}_{kl} - \epsilon^{tr}_{kl}) + (1-\xi)C^A_{ijkl}\epsilon^o_{kl} = 0 \tag{3.27}$$

ϵ^o_{kl} indicates the effect of inclusions on each other and it is the average strain in the surrounding medium composed of other inclusions and matrix. It is important that ϵ^a_{kl} which is applied strain due to linear elastic fracture mechanics solution is replaced by ϵ^o_{kl} which also takes other inclusion effects into account.

The unknowns in this problem are ϵ^o_{kl} and ϵ^*_{mn}. Using the previous equations to solve for ϵ^o_{kl} and putting $\xi = 0.99$ the following expressions are obtained:

$$\epsilon^o_{kl} = (C^A)^{-1}_{klij}\left[0.99C^A_{ijmn}(I_{mnrs} - S_{mnrs})(\epsilon^{tr}_{rs} + \epsilon^{**}_{rs})\right] \tag{3.28}$$

where I_{mnrs} is 4^{th} order identity tensor:

$$I_{mnrs} = \frac{1}{2}(\delta_{mr}\,\delta_{ns} + \delta_{ms}\,\delta_{nr}) \tag{3.29}$$

$$\epsilon_{kl}^{**} = ((\boldsymbol{C^M}+\boldsymbol{C^A})\boldsymbol{S}-\boldsymbol{C^A})^{-1}_{klmn}\Big[(\boldsymbol{C^A}-\boldsymbol{C^M})_{mnrs}\epsilon^{o}_{rs}+((\boldsymbol{C^A}-\boldsymbol{C^M})\boldsymbol{S}+(\boldsymbol{C^M}-\boldsymbol{C^A}))_{mnrs}\epsilon^{tr}_{rs}\Big] \tag{3.30}$$

where boldfaced expressions are tensors . Imposing plane strain conditions leads to new transformation strains as the following by Lambropoulos [58] formulation.

$$E^{tr}_{11} = \big(1+\frac{\nu}{3}\big)\epsilon^{*}_{11}+\nu\epsilon^{*}_{22} \tag{3.31}$$

$$E^{tr}_{22} = \big(1+\frac{\nu}{3}\big)\epsilon^{*}_{22}+\nu\epsilon^{*}_{11} \tag{3.32}$$

$$E^{tr}_{12} = \epsilon^{*}_{12} \tag{3.33}$$

Then for Mode I, crack tip stress intensity factor change due to martensite transformation can be found by integrating Hutchinson's expression [57]:

$$\begin{aligned} dK^{tip} = \frac{1}{\sqrt{8\pi}}\frac{EdA}{1-\nu^2}r^{-\frac{3}{2}}\big[(E^{tr}_{11}+E^{tr}_{22})\cos\big(\frac{3\beta}{2}\big)+3E^{tr}_{12}\cos\big(\frac{5\beta}{2}\big)\sin(\beta)+... \\ ...\frac{3}{2}(E^{tr}_{22}-E^{tr}_{11})\sin(\beta)\sin\big(\frac{5\beta}{2}\big)\big] \end{aligned} \tag{3.34}$$

where $\iint_A dK^{tip} = \Delta K^{tip} = K^{\infty} - K^{tip}$.

To evaluate this integral, an iteration schematic was necessary since the integral domain depends on r_c which is also dependent on K^{tip}. The resultant K^{tip} values due to transformation toughening can be summarized in the following table.

Table 3.4. Stress intensity values for specific far field applied tensile stress values in case of no transformation.

σ^{∞}	$\frac{a}{B} = 0.5$
20 MPa	22.3 MPa$\sqrt{m}$
30 MPa	33.4 MPa$\sqrt{m}$
40 MPa	44.6 MPa$\sqrt{m}$
50 MPa	55.8 MPa$\sqrt{m}$

Table 3.5. Stress intensity values for specific far field applied tensile stress values in case of fully martensite transformation.

σ^{∞}	$\frac{a}{B} = 0.5$
20 MPa	21.4 MPa$\sqrt{m}$
30 MPa	32.4 MPa$\sqrt{m}$
40 MPa	43.3 MPa$\sqrt{m}$
50 MPa	54.2 MPa$\sqrt{m}$

ΔK^{tip} values are listed in the following table .

Table 3.6. Decrease in stress intensity values for specific far field applied tensile stress values in case of fully martensite transformation.

σ^{∞}	$\frac{a}{B} = 0.5$
20 MPa	0.9 MPa$\sqrt{m}$
30MPa	1.0 MPa$\sqrt{m}$
40 MPa	1.3 MPa$\sqrt{m}$
50 MPa	1.6 MPa$\sqrt{m}$

As can be seen from K^{tip} values after the martensite formation, these are nearly equal to K^{∞} values. This seems to result from the fact that averaging all variant strains does not produce any toughening effect.

Another important factor is crystallographic orientation. Lu *et al.* [56] used 25 points on crystallograpic projection plane to model isotropic NiTi behaviour in Lagoudas *et al.* [61]. Assuming the points are equally spaced for each row (The coordinates of these points are not given explicitly in this paper [56]), crystallographic orientation matrices are found in order to transform transformation strain to global coordinates. The following figure shows the distribution of these points by streographic projection:

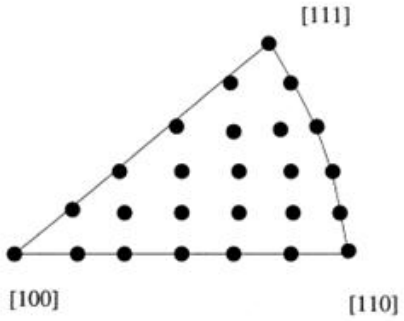

Figure 3.13. Streographic projection of grain orientations forming up the martensite zone ahead of crack tip [56].

The following table shows stress intensity factor decrease due to transformation toughening.

Table 3.7. Decrease in stress intensity values for specific far field applied tensile stress values in case of fully martensite transformation considering also orientation and variant effects.

σ^{∞}MPa	ΔK^{tip} MPa$\sqrt{m}$	K^{∞} MPa$\sqrt{m}$	K^{tip}MPa$\sqrt{m}$
20	9	22.3	13.3
30	13.6	33.5	19.9
40	18.1	44.6	26.5
50	22.6	55.8	33.2

The following graphs show fully transformed martensite zone with respect to different σ^{∞} 's.

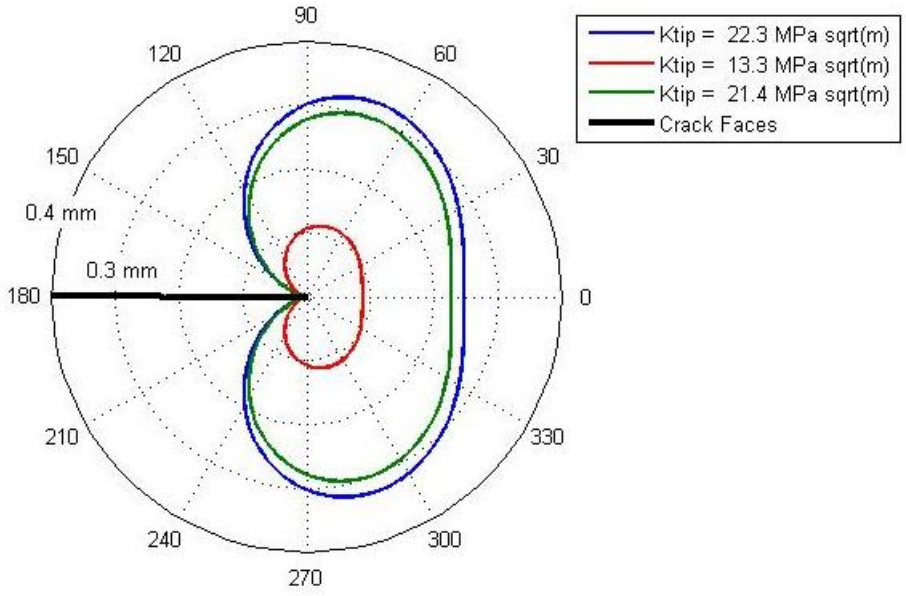

Figure 3.14. Fully martensite zone boundary at $\sigma^{\infty} = 20$ MPa.

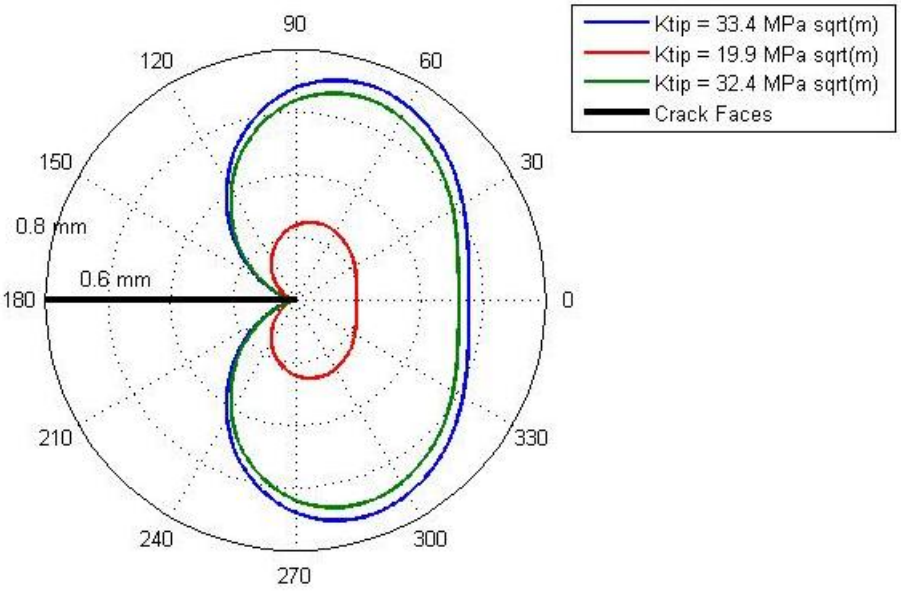

Figure 3.15. Fully martensite zone boundary at $\sigma^{\infty} = 30$ MPa.

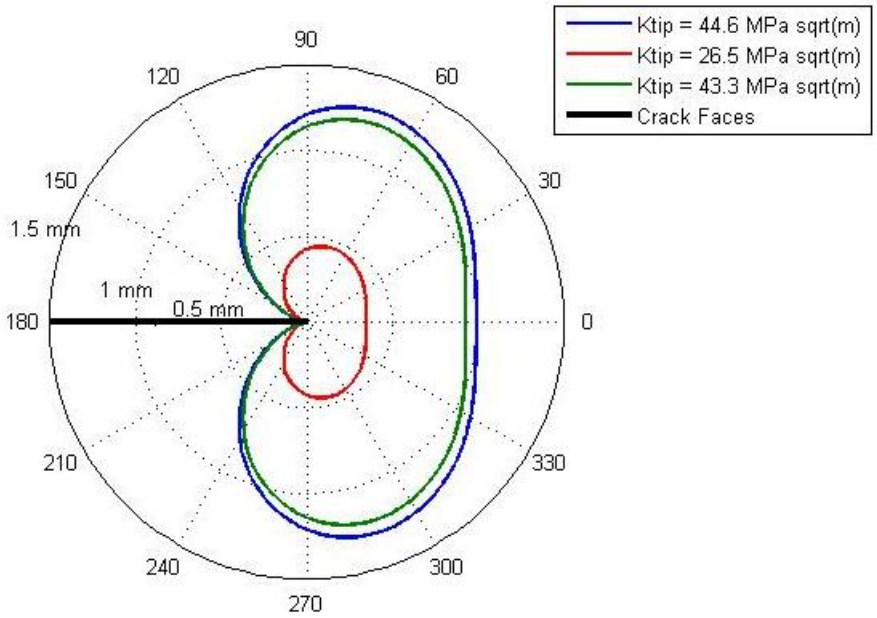

Figure 3.16. Fully martensite zone boundary at $\sigma^{\infty} = 40$ MPa.

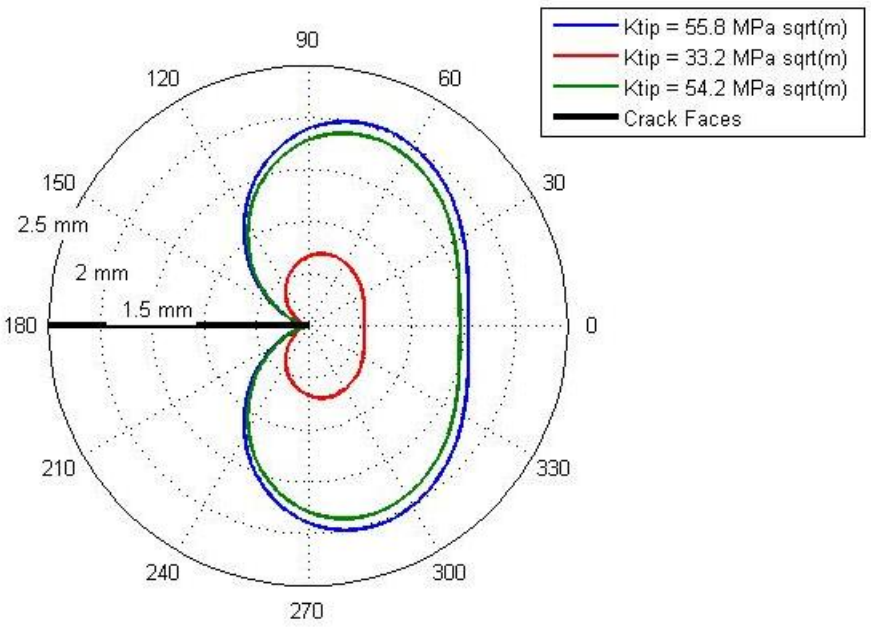

Figure 3.17. Fully martensite zone boundary at $\sigma^{\infty} = 50$ MPa.

4. CONCLUSION

In this study, calculation of stress intensity factor at the crack tip of an edge cracked shape memory alloy plate subjected to Mode I loading under uniform far field stress is presented. J integral was explicitly implemented for shape memory alloys by using Auricchio *et al.*'s [21-22] constitutive model. It was shown that in martensite zone J values decrease as one gets away from crack tip. J values in fully austenite zone are seen to be nearly constant. J contour integrals evaluated by ABAQUS's own algorithm gives constant values in austenite zone as well. They are decreasing in fully martensite zone as one gets away from crack tip. In the study of Miray Şimşek [49] this was also confirmed by using ABAQUS. The decreasing trend in fully martensite zone must be confirmed in other geometries and loading conditions for cracks.

Using E_{tip} to calculate stress intensity factor from J integral evaluated on a contour very close to crack tip, decreases from 55.8 and 33.5 MPa$\sqrt{m}$ to 38.9 and 22.3 MPa$\sqrt{m}$ are obtained respectively. This results from transformation toughening because some of external work on cracked shape memory alloy specimen used for transformation phenomenon. Whether the relationship used between J and K_I holds for shape memory alloys as it does in LEFM should be confirmed in future studies by experimentally measuring strain field, determining transformation strain from orientation distribution and variants, and finally calculating J integral on contours very close to the crack tip.

In some models in literature, deformation plasticity are used while deriving the constitutive model . This deformation plasticity assumption that brings in proportional loading makes equations to be solved analytically. In order to compare deformation plasticity based models such as Maletta *et al.* [50-52] and Auricchio *et al.*'s constitutive model [21-22]; Budiansky's criteria [53] for applicability of deformation plasticity were used. As shown in Section 2.3 according to Budiansky criteria, there is considerable amount of difference in terms of proportionality of loading between these two models. This analysis showed that these two approaches can not be used

interchangibly. Thus, these two approaches will result in different values in terms of stress, strain and volumetric martensite fraction near the crack tip.

In Chapter 3, micromechanical approaches for transforming materials problems are tried to be adopted for fracture mechanics of shape memory alloys. Firstly Yi & Gao's approach [24] was implemented by using Auricchio *et al.*'s constitutive model [21-22]. Extracted transformation strains in fully martensite zone was plugged into Eshelby inclusion method [27] and the resultant expression combined with Rice weight function for plane stress [29]. Transformation toughnening tried to be quantified. However, this method shows large discrepancy between ABAQUS results. This may be due to the fact that Auricchio *et al.*'s model [21-22] is a plasticity based model and is not based on micromechanical arguments.

As another approach, transformation strain for NiTi was evaluated from Lu *et al.* [60] and plugged into the expression derived by Mori-Tanaka averaging method for plane strain . In this method the effects of other inclusions is considered by ϵ^o_{kl}. The effect of geometry controls which variant would be active and in return determines the average of transformation strain in the fully transformed zone. The effect of inclusions on stress intensity factor is calculated by Hutchinson's equation [57]. There are 2 different orientation distributions considered in this text. First one is taking all inclusion principal axes coinciding with macro coordinate system. Secondly, Lu *et al.*[56] has given an orientation distribution to model polycrystal behaviour. The former one didn't result considerable amount of transformation toughening. The latter one has been evaluated to give more than significant transformation toughnening. As a result the effect of orientation distribution of polycrystal NiTi, which results from different grain orientations, was shown.

First result of this study is that J contour integral is path dependent in martensitic zone at the crack tip. However, it remains constant in austenitic zone. Secondly, numerical calculations and micromechanical approaches indicate that there is decrease in stress intensity factor because of transformation toughening. Also, orientation effects near the crack tip are significant in order to quantify this decrease in stress intensity

factor. If transformation strain components are favorable due to orientation distribution of grains, significant decrease in opening stress level can be observed. However, this effect should be confirmed by experiments in different loading conditions by finding orientational distribution of grains near the crack tip and variants formed in those due crack tip stress field interaction in the future studies.

REFERENCES

1. Çopur, H., *Crack Initiation in Statically Loaded Functionally Graded Materials*, M.S. Thesis , Bogazici University, 2004.

2. Goldstein, D., "A Source manual for Information on NITINOL and NiTi", *Naval Surface Weapon Center Research and Technology Department Report*, 1978.

3. Buehler, W.J., and R.C. Wiley, "Nickel Base Alloys", *US Patent Office* , 3174851, 1965.

4. Lagoudas, D., *Shape Memory Alloys:Modeling and Engineering Applications*, Springer, New York, 2008.

5. Bhattacharya, K., *Microstructure of Martensite*, Oxford University Press, New York, 2007.

6. Müller, I., "Pseudoelasticity In Shape Memory Alloys: An Extreme Case of Thermoelasticity" , *Inst. for Mathematics and its Applications Report*, University of Minnesota, 1985.

7. Müller, I., and H. Xu, "On the Pseudo-Elastic Hysteresis", *Acta Metallurgica et Materialia* , Vol. 39, No. 3, pp. 263-271, 1991.

8. Anderson, T.L., *Fracture Mechanics: Fundamentals and Applications*, CRC Press, 2^{nd} Edition, pp.96-97, 1995.

9. Williams, M.L., "On the Stress Distribution at the Base of a Stationary Crack", *Journal of Applied Mechanics* , Vol. 24 , pp. 109-114, 1957.

10. Westergaard, H.M., "Bearing Pressures and Cracks", *Journal of Applied Mechanics*, Vol.6, pp. 49-53, 1939.

11. Rice, J.R., "A path independent integral and the approximate analysis of strain concentration by notches and cracks ", *Department of Defense Advanced Research Projects Agency Contract SD - 86 Material Research Program Report E39*, 1967.

12. Hertzberg, R., *Deformation and Fracture Mechanics of Engineering Materials*, Wiley, 4^{th} Edition, pp. 360, 1996.

13. Eischen, J.W., "Fracture of nonhomogeneous materials", *International Journal of Fracture*, Vol. 34, pp. 3-22, 1987.

14. Anlas, G., M.H. Santare, and J. Lambros, "Numerical Calculation of Stress Intensity Factors in Functionally Graded Materials", *International Journal of Fracture*, Vol.104, pp. 131-143, 2000. *International Journal of Solids and Structures*, Vol. 48, pp. 1658-1664, 2011.

15. Gollerthan, S., M.L. Young, A. Baruj, J. Frenzel, W.W. Schmal, and G. Eggeler, "Fracture mechanics and microstructure in NiTi shape memory alloys", *Acta Materialia* , Vol. 57, pp. 1015-1025, 2009.

16. American Society for Testing and Materials (ASTM), "Standard Test Method for Linear-Elastic Plane Strain Fracture Toughness K_{Ic} of Metallic Materials E 399", 2004.

17. Daymond, M.R., M.L. Young, J.D. Almer, and D.C. Dunand, "Strain and texture evolution during mechanical loading of a crack tip in martensitic shape memory NiTi", *Acta Materialia*, Vol. 55, pp. 3929-3942, 2007.

18. Birman, V., "On mode I fracture of shape memory alloy plates", *Smart Materials and Structures Journal* , Vol. 7, pp. 433-437, 1998.

19. Tanaka, K., "A Thermomechanical Sketch of Shape Memory Effect: One Dimensional Tensile Behaviour", *Res Mechanica Journal* , Vol. 18, pp. 251-263, 1986.

20. Wang, X.M., Y.F. Wang, A. Baruj, G. Eggeler, and Z.F. Yue, "On the formation of martensite in front of cracks in pseudoelastic shape memory alloys", *Materials Science and Engineering A*, Vol. 394, pp. 393-398, 2005.

21. Auricchio, F., R.L. Taylor, and J. Lubliner, "Shape memory alloys :macromodelling and numerical simulations of the superelastic behavior", *Computer Methods in Applied Mechanics and Engineering*, Vol. 146, pp. 281-312, 1997.

22. Hibbitt, D., B. Karlsson, and P. Sorensen, *ABAQUS UMAT Subroutine, ABAQUS Standard User's Manual*, Dassault Systems, Rhode Island, 2001.

23. Wang, G.Z., "Effects of notch geometry on stress-strain distribution, martensite transformation and fracture behaviour in shape memory alloy NiTi", *Materials Science and Engineering A*, Vol. 434, pp. 269-279, 2006.

24. Yi, S., and S. Gao, "Fracture toughening mechanism of shape memory alloys due to martensite transformation", *International Journal of Solids and Structures*, Vol.37, No. 38, pp. 5315-5327, 2000.

25. Sun, Q.P., and K.C. Hwang, "Micromechanics modelling for the constitutive behavior of polycrystalline shape memory alloys–I, Derivation of general relations", *Journal of the Mechanics and Physics of Solids* , Vol. 41, No. 1, pp. 1-17, 1993.

26. Sun, Q.P., and K.C. Hwang, "Micromechanics modelling for the constitutive behavior of polycrystalline shape memory alloys–II, Study of the individual phenomena", *Journal of the Mechanics and Physics of Solids*, Vol. 41, No. 1, pp. 19-33, 1993.

27. Eshelby, J.D., "The determination of the elastic field of an ellipsoidal inclusion, and related problems", *Proceedings of the Royal Society of London, Series A, Mathematical and Physical Sciences* , Vol. 241, pp. 376-396, 1957.

28. Evans, A.G., and A.H. Heuer, "Review–Transformation toughening in Ceramics: Martensitic Transformations in Crack-Tip Stress Fields", *Journal of American Ce-*

ramic Society, Vol. 63, pp. 241-248, 1980.

29. Rice, J.R., "Some Remarks on Elastic Crack-Tip Stress Fields", *International Journal of Solids and Structures*, Vol. 8, pp. 751-758, 1972.

30. Yi, S., S. Gao, and L. Shen, "Fracture Toughening Mechanism of Shape Memory Alloys under Mixed Mode Loading due to Martensite Transformation", *International Jounal of Solids and Structures*, Vol. 38, pp. 4463-4476, 2001.

31. Yan, W., C.H. Wang, X.P. Zhang, and Y-W. Mai, "Effect of Transformation Volume Contraction on the Toughness of Superelastic Shape Memory Alloys", *Smart Materials and Structures* , Vol. 11, pp. 947-955, 2002.

32. Fang, D-N, W. Lu, W. Yan, T. Inoue, and K.C. Hwang, "Stress Strain Relation of CuAlNi SMA single Crystal under Biaxial Loading – Constitutive Model and Experiments", *Acta Materialia*, Vol. 47, pp. 269-280, 1999.

33. Freed, Y., and L. Sills-Banks, "Crack Growth Resistance of Shape Memory Alloys by Means of a Cohesive Zone Model", *Journal of the Machanics and Physics of Solids* , Vol. 55, No. 10, pp. 2157-2180, 2007.

34. Panoskaltsis, V.P., S. Bahuguna, and D. Soldatos, "On the Thermomechanical Modeling of Shape Memory Alloys", *International Journal of Nonlinear Mechanics*, Vol. 39 , No. 5, pp. 709-722, 2004.

35. Ma, L., "Fundamental Formulation for Transformation Toughening", *International Journal of Solids and Structures* , Vol. 47, pp. 3214-3220, 2010.

36. Lexcellent, C., and F. Thiebaud, "Determination of the Phase Transformation Zone at a Crack tip in a Shape Memory Alloy Exhibiting Asymmetry between Tension and Compression", *Scripta Materialia* , Vol. 59, pp. 321-323, 2008.

37. Bouvet, C., S. Calloch, and C. Lexcellent, "A Phenomenological Model for Pseu-

doelasticity for Shape Memory Alloys under Multiaxial Proportional and Nonproportional Loadings", *European Journal of Mechanics A/Solids* , Vol. 23, pp. 37-61, 2004.

38. Taillard, K., S.A. Chirani, S. Calloch, and C. Lexcellent, "Equivalent Transformation Strain and Its Relation with Martensite Volume Fraction for Isotropic and Anisotropic Shape Memory Alloys", *Mechanics of Materials* , Vol. 40, pp. 151-170, 2008.

39. Laydi, M.R., and C. Lexcellent, "Yield Criteria for Shape Memory Materials: Convexity Conditions and Surface Transport", *Mathematics and Mechanics of Solids*, Vol. 15, No. 2, pp. 165-208, 2010.

40. Robertson, S.W., A. Mehta, A.R. Pelton, and R.O. Ritchie , "Evolution of Crack-Tip Transformation Zones in Superelastic Nitinol Subjected to In Situ Fatigue: A Fracture Mechanics and Synchrotron X-Ray Microdiffraction Analysis", *Acta Materialia*, Vol. 55, pp. 6198-6207, 2007.

41. Lexcellent, C., M.R. Laydi, and V. Taillebot, "Analytical Prediciton of the Phase Transformation Onset Zone at a Crack Tip of a Shape Memory Alloy Exhibiting Asymmetry between Tension and Compression", *International Journal of Fracture*, Vol. 169, pp. 1-13, 2011.

42. Daly, S. H., *Deformation and Fracture of Thin Sheets NITINOL*, PhD. Thesis, California Institute of Technology, 2007.

43. Mura, T., *Micromechanics of Defects in Solids*, Martinus Nijhoff, Dordrecht, 1987.

44. Hellen, T.K., "On the Method of Virtual Crack Extensions", *International Journal for Numerical Methods in Engineering* , Vol. 9, pp. 187-207, 1975.

45. Hellen, T.K., "Virtual Crack Extension Methods for Nonlinear Materials", *International Journal for Numerical Methods in Engineering* , Vol. 28, pp. 929-942,

1989.

46. Parks, D.M, "The Virtual Crack Extension Method for Nonlinear Material Behavior", *Computer Methods in Applied Mechanics and Engineering* , Vol. 12, pp. 353-364, 1977.

47. DeLorenzi, H.G., "Energy Release Rate Calculations by the Finite Element Method", *Engineering Fracture Mechanics Method* , Vol. 21, No. 1, pp. 129-143, 1985.

48. Shih, C.F., B. Moran, and T. Nakamura, "Energy Release Rate along a Three Dimensional Crack Front in a Thermally Stressed Body", *International Journal of Fracture* , Vol. 30, pp. 79-102, 1986.

49. Şimşek, M., *Fracture Mechanics Analysis of Shape Memory Alloys Using Finite Elements*, M.S. Thesis, Bogazici University, 2009.

50. Falvo, A., F. Furgiuele, A. Leonardi, and C. Maletta, "Stress Induced Martensitic Transformation in the Crack Tip Region of a NiTi Alloy", *Journal of Materials Engineering and Performance*, Vol. 18, pp. 679-685, 2009.

51. Maletta, C., and F. Furgiuele, "Analytical modeling of stress induced martensitic transformation in the crack tip region of nickel-titanium alloys", *Acta Materialia*, Vol. 58, pp. 92-101, 2010.

52. Maletta, C., and F. Furgiuele, "Fracture control parameters for NiTi based shape memory alloys ", *International Journal of Solids and Structures*, Vol. 48, pp. 1658-1664, 2011.

53. Budiansky, B., "Reassessment of deformation theories of plasticity", *Journal of Applied Mechanics*, Vol. 26, pp. 259-264, 1959.

54. Wechsler, M.S., and D.S. Lieberman, T.A. Read, "On the Theory of Formation of

Martensite", *Transactions of the American Institute of Mining, Metallurgical and Petroleum Engineers*, Vol. 197, pp. 1503-1515, 1953.

55. Khachaturyan, A.G., *Theory of Structural Transformations in Solids*, Wiley, New York, 1983.

56. Lu, Z.K.,and G.J. Weng, "A Self-Consistent Model for the Stress-Strain Behavior of Shape Memory Alloy Polycrystals", *Acta Materialia* , Vol. 46, No. 15, pp. 5423-5433, 1998.

57. Hutchinson, J.W., "On Steady Quasi-Static Crack Growth", *Air Force Office of Scientific Research Report* , 1974.

58. Lambropoulos, J.C., "Shear, Shape, Orientation Effects in Transformation Toughnening", *International Journal of Solids and Structures* , Vol. 22, No. 10, pp. 1083-1106, 1986.

59. Schmid, E., and W. Boas, *Plasticity of Crystals with Special Reference to Metals*, F.A. Hughes & Co. Limited, London, 1950.

60. Lu, Z.K., and G.J. Weng, "Martensitic Transformation and Stress-Strain Relations of Shape Memory Alloys", *Journal of the Mechanics and Physics of Solids* , Vol. 45, No. 11-12, pp. 1905-1928, 1997.

61. Lagoudas, D.C., J.G. Boyd, and Z. Bo, "Micromechanics of Active Composites with SMA Fibers", *Journal of Engineering Materials and Technology* , Vol. 116, pp. 337-347, 1994.